



The Globally Coherent Pattern of Autumn Monsoon Precipitation

Nandini Ramesh*, Quentin Nicolas

Department of Earth and Planetary Science, University of California, Berkeley, California

William R. Boos

Department of Earth and Planetary Science, University of California, Berkeley, California

Climate and Ecosystem Sciences Division, Lawrence Berkeley National Laboratory, Berkeley, California

*Corresponding author: Nandini Ramesh, nandini.ramesh@sydney.edu.au.

ABSTRACT

Over most tropical land areas, the annual peak in precipitation occurs during summer, associated with the local monsoon circulation. However, in some coastal regions in the tropics the bulk of annual precipitation occurs in autumn, after the low-level summer monsoon westerlies have abated. Examples include the Nordeste region of Brazil, southeastern India and Sri Lanka, and coastal Tanzania. Unlike equatorial regions, they receive little rainfall during local spring. Such regions are present along the eastern coasts of nearly all continents, suggesting that they comprise a coherent yet previously unrecognized global phenomenon.

In this study, we identify eight tropical locations that experience an “autumn monsoon” and show that this unusual seasonal cycle is generated by similar mechanisms in all of these. When these regions receive their peak rainfall, they lie poleward of the ITCZ in easterly low-level winds. The spatial structure of precipitation in these regions can be explained by their placement to the east of mountain ranges that organize moist convection on their windward sides. However, orographic forcing alone cannot explain their unique seasonal cycle: despite similarities in wind direction, surface humidity, and sea surface temperatures (SSTs) between autumn and spring, these regions receive significantly more rainfall in autumn than in spring. We show that this is due to differences in the large-scale atmospheric stability between the equinoctial seasons, which can be captured by a relative SST metric and is influenced by SSTs in the remote eastern upwelling zones of the Pacific and Atlantic Oceans.

1. Introduction

Land regions throughout the tropics typically experience peak rainfall during summer, associated with monsoon circulations on each landmass. However, on multiple continents, areas exist where most of the annual precipitation occurs in autumn or winter, and the summer is relatively dry. Unlike locations close to the equator that experience two rainy seasons in spring and autumn, such as the equatorial parts of Africa and South America, these regions receive comparatively little precipitation during spring.

A well-studied example of such a location is the Nordeste region of Brazil, where the wet season occurs in austral autumn. In South Asia, the autumn rainfall peak is referred to as the northeast monsoon, retreating monsoon, or post-monsoon, and is the primary source of rainfall for southeastern peninsular India and northeastern Sri Lanka. There are also regions that receive much of their annual precipitation during local autumn in East Africa, Southeast Asia, and Central America.

Figure 1 displays the climatological fraction of total annual rainfall received during autumn and winter in the tropics of each hemisphere. Regions that receive half or more of their annual rainfall in these months (September to February in the Northern Hemisphere, or March to August in the Southern Hemisphere) are typically narrow strips along the eastern coasts of landmasses or island chains. In most cases, they are located to the east and equatorward of the summer monsoon regions on each continent.

In previous studies that classified the tropics into climatic regimes, these regions have either been categorized as semiarid savannas or grouped with summer monsoon regions (Ramage et al. 1971; Wang 1994; Zhang and Wang 2008; Beck et al. 2018), possibly due to the relatively low spatial resolution of historical precipitation data. However, the unusual seasonal cycle of these regions has long been known, as noted in the book *The Earth's Problem Climates* (Trewartha 1961), which

refers to an annual “summer drought” in several of these areas when cataloguing the locations on each continent with climatological characteristics that do not conform to those of their surroundings. Most of these areas are densely populated, and some have historical records detailing drought-induced famines of devastating intensity, including Brazil’s Nordeste region, southeastern India, the island of Luzon in the Philippines, and southern coastal Kenya (Davis 2002). Despite the striking similarities between the climates of these regions, they have not previously been considered as a unified phenomenon or climate regime with comparable physical drivers. In this study, we propose on the basis of observed features and physical arguments that these regions constitute a single climate type or regime, generated by similar mechanisms.

a. Review of studies of individual regions

Although no work has proposed a unified view of all of these regions, the annual cycle and variability of precipitation in many of these locations have been examined in regional studies. Below, we summarize these existing studies.

Of the autumn monsoon regions, the case that has received perhaps the most attention is the Nordeste region of Brazil (Hastenrath 2012), an area that typically receives its peak rainfall in April, i.e., austral autumn, in contrast with the summer (December–February) peak in rainfall experienced by most of the South American landmass in the Southern Hemisphere. This region is prone to severe droughts known as *secas* that have had pronounced socioeconomic impacts, resulting in famines and mass migrations out of the region (Greenfield 2001; Davis 2002; Aceituno et al. 2009); and is home to large urban centers such as Recife and Salvador. The timing of the annual rainfall peak in the northern part of this region has been attributed to the location of the Intertropical Convergence Zone (ITCZ) in the Atlantic sector, which reaches the southernmost point in its annual migration in March and April (Hastenrath 2012); we will show

that additional factors play a significant role. The interannual variability here is closely related to El Niño-Southern Oscillation (ENSO) (Pezzi and Cavalcanti 2001), which influences the timing of the ITCZ's meridional movement via the Atlantic sea surface temperature (SST) gradient (Nobre and Shukla 1996; Uvo et al. 1998; Giannini et al. 2004).

In the Northern Hemisphere, the Maracaibo region of northern Venezuela and Colombia similarly experiences an autumn peak in rainfall, in contrast with surrounding summer-monsoon regions (Pulwarty et al. 1992), and is heavily influenced by tropical Pacific SSTs (Lyon 2003). Parts of the Caribbean coast of Central America, including northern Honduras (Portig 1965) and the flood-prone Mexican state of Tabasco (Aparicio et al. 2009), also receive most of their rainfall in autumn.

A number of eastern coastal regions in the Indo-Pacific display a similar seasonal cycle. In South Asia, the autumn rainfall peak over densely populated southeastern peninsular India and Sri Lanka provides a crucial source of water for rice cultivation (referred to as the *rabi* and *maha* crops, respectively, in these two countries; Singh and Sontakke 1999; Zubair 2002). This rainfall is highly variable on interannual timescales: both flooding due to excessive rainfall (van Oldenborgh et al. 2016; Kumaran et al. 2020) and droughts (Guha-Sapir et al. 2016) have afflicted the region in recent years. ENSO is a key modulator of this variability (Suppiah 1989; Zubair 2002; Kumar et al. 2006), along with SSTs in the Indian Ocean (Zubair et al. 2003; Kripalani and Kumar 2004; Yadav 2013). Similarly to the Nordeste region of Brazil, it has been hypothesized that the ITCZ's meridional movement determines the timing and amount of rainfall over this part of the world (Yadav 2013; Gadgil 2018).

Figure 1 shows that parts of the Maritime Continent and Southeast Asia receive most of their rainfall in autumn and winter. Exceptions to the general pattern of summer rainfall maxima in this region have been noted in several studies (e.g., Wang 1994; Chang et al. 2004, 2005). Of these

exceptions, coastal central Vietnam and the eastern halves of the Malay Peninsula and Philippines stand out as locations that receive significantly more rainfall in autumn and winter than in spring and summer (Chang et al. 2005; Robertson et al. 2011), and the latter two of these have been described as northward extensions of the Australian summer monsoon (Robertson et al. 2011). The anticyclonic winter monsoon circulation over East Asia is known to bring severe weather to parts of subtropical East Asia (e.g., Chang et al. 2006), which may contribute some of the observed rainfall; however, studies of the areas of Vietnam and the Malay Peninsula highlighted in Figure 1 have emphasized that the peak rainfall occurs during the transition from the summer to winter monsoons, i.e., in autumn (Yokoi and Matsumoto 2008; Chen et al. 2012, 2013). Numerous studies have pointed out that the transitions between the Asian and Australian summer monsoons are not symmetric: the ITCZ moves southwards gradually from Asia to Australia over the course of boreal autumn, but abruptly shifts northwards from Australia to Asia in boreal spring (Wang 1994; Aldrian and Susanto 2003; Hung et al. 2004; Chang et al. 2005; Zhang and Wang 2008). Consequently, the boreal autumn and winter months bring a peak in rainfall to a few locations in the Maritime Continent that are north of the equator, but equivalent regions on the other side of the equator that receive peak rainfall in austral autumn and winter are far less extensive. This is consistent with Figure 1, which shows that the eastern coastal regions of Australia and the island of New Guinea do not receive more rainfall in local autumn and winter than in spring and summer. One hypothesis for the mechanism producing this asymmetry is that the Pacific Walker cell, which is maintained by the zonal SST gradient across the equatorial Pacific, is strongest in boreal autumn due to enhanced upwelling in the eastern equatorial Pacific at this time of year producing cool SSTs, leading to increased ascent over the Maritime Continent (Wang 1994; Li and Philander 1996). A later hypothesis, put forward by Chang et al. (2005) and explored in model experiments by Wang and Chang (2008), proposes that the high heat capacity of the oceans leads to warm SSTs

in the autumn hemisphere following the peak summer insolation; that effect, in combination with the shape and location of the landmasses in the region, which are cooler in autumn due to their low heat capacity, gives rise to sea level pressure gradients that favor convergence and rainfall over a larger area in autumn and winter than during spring.

At the other end of the Indian Ocean basin, the Tanzanian and southern Kenyan coastline receives maximum precipitation in the austral autumn months of April and May. This rainy season is known locally as the *masika* or “long rains,” and is the primary source of rainfall for major population centers such as Dar Es Salaam and Mombasa. Much of East Africa experiences a season of “long rains” during austral autumn and “short rains” during austral spring, but the coastal section of East Africa in the Southern Hemisphere is the only area where the *masika* rains comprise more than half of the annual rainfall (Hastenrath et al. 2011; Yang et al. 2015; Gamoyo et al. 2015; Camberlin and Planchon 1997). The region is highly vulnerable to variations in this rainfall: shortfalls have led to famines in greater East Africa (e.g., Lyon and DeWitt 2012), and excessive rainfall has produced flooding in Dar Es Salaam in recent years (Guha-Sapir et al. 2016).

b. Goals and approach

In this study, we examine the mechanisms that generate the autumn rainfall peak in all of the regions discussed above and provide evidence that they comprise an analogous phenomenon on various continents, driven by similar processes.

We begin by examining the spatial distribution of regions in the tropics that receive most of their annual rainfall in autumn and winter, as opposed to summer (Section 3). We find strong parallels between these regions in terms of the timing of the annual precipitation peak and their alignment with the eastern margins of landmasses. We then investigate three factors that typically affect the

annual cycle of tropical precipitation. The first is the seasonal movement of the ITCZ: as summer monsoons on each continent end, the ITCZ moves equatorward in autumn, possibly producing peak rainfall in locations that lie equatorward of nearby summer monsoon regions (Section 4). We find that this does not explain the autumn monsoon pattern, as the autumn monsoon regions do not lie within the main ITCZ during the months of peak rainfall; instead, they manifest as narrow protrusions from the main rainband into the autumn hemisphere. A significant feature associated with the seasonal movement of the ITCZ is the reversal of the prevailing winds from westerly during local summer, when the ITCZ is poleward of the autumn monsoon regions, to easterly during the months of peak precipitation. These easterly winds and the proximity of the autumn monsoon regions to mountain ranges, as well as previous work on some of these regions (e.g., Lyra et al. 2014; Chang et al. 2016), lead us to consider the second factor: the interaction of winds with orography to produce rainfall (Section 5). We find that orographic effects broadly explain the spatial distribution of rainfall in autumn, especially the alignment of autumn monsoon regions along eastern coasts, but do not provide accurate estimates of the rainfall amount or of the annual cycle. The third factor we investigate is the role of moist convection. Using a budget analysis, we show that horizontal moisture convergence associated with deep, convectively coupled ascent above orography in these regions is responsible for the large rainfall amounts observed during autumn (Section 6). Further, we find that the effects of local and remote SSTs, particularly in eastern ocean upwelling zones, play a key role in setting the atmospheric conditions that promote moist convection in autumn (Section 7). We summarize our results and their implications in Section 8.

The focus of this study is the large-scale, seasonal-mean setting that facilitates the observed autumn peak in precipitation. While synoptic-scale phenomena and extreme rainfall events have been documented in these regions, they do not constitute the primary source of rainfall during

autumn. We provide a summary of previous work on these extreme events as well as evidence that these regions experience consistent rainfall through the autumn in the Supplemental Material.

2. Data and Methods

We use multiple observational and reanalysis data sets, all of which are publicly available. Table 1 lists the name, resolution, geographic coverage, time period, and variables used for each data set. Where variables from different data sources are shown together, climatologies and other quantities are calculated for the overlapping set of years. All data analyzed is at monthly resolution, with the exception of daily rainfall data used in the Supplemental Material. While monthly data cannot capture certain features of the autumn monsoon such as precise onset dates and individual synoptic events, we use monthly data to investigate the seasonal-mean conditions of interest in this study. A more detailed examination of features requiring higher temporal resolution will be conducted in future work.

Our figures and analysis are produced using two precipitation estimates: TRMM and CHIRPS, which have differing temporal coverage and spatial resolution. Importantly, CHIRPS only contains data over land, whereas TRMM contains data over both land and ocean. In computing time series or other spatial averages, the averaging is performed within the boxes shown in Figure 3 with areas outside the 0.5 contour in these figures masked to exclude regions that receive less than half of their annual rainfall in autumn and winter. Smaller boxes shown in Figures 1, 4, 5, and 6 contain the same masked land area as those shown in Figure 3 and were used for visualization.

For our moisture budget analysis and visualization of wind fields, we used the most recent version of the European Center for Medium-Range Weather Forecasts Reanalysis (ERA5). This version is at a higher resolution than previous generations, making it more appropriate for use in regions with

topography, and assimilates data from multiple scatterometer products, resulting in an improved representation of the surface winds when compared with observations (Hersbach et al. 2020).

3. The Climatological Distribution of Tropical Autumn Precipitation

Figure 1 displays the climatological fraction of annual rainfall over tropical land regions during autumn and winter in each hemisphere, here defined as September to February for the Northern Hemisphere and March to August for the Southern Hemisphere, computed using the CHIRPS data. Regions that receive most of their annual rainfall in summer (shaded blue) cover most of this map, consistent with the dominant role played by summer monsoon circulations in producing rainfall over tropical land. Most regions that receive half or more of their annual rainfall during autumn and winter (shaded orange and red) are along the eastern coasts of continents and in many cases lie equatorward of a large summer monsoon region.

We select the following eight eastern coastal regions (highlighted by boxes in Figure 1) that receive most of their annual rainfall in autumn and winter for analysis in this study:

1. Central America: northern Honduras and the coast of Tabasco in Mexico.
2. Venezuela: the Maracaibo region of northern Venezuela and Colombia.
3. South Asia: eastern Sri Lanka and the southeastern Indian state of Tamilnadu.
4. Malay Peninsula: the southeastern edge of the Malay Peninsula.
5. Vietnam: central coastal Vietnam.
6. Philippines: the eastern half of the Philippines.
7. Brazil: northeastern coastal Brazil, known as the Nordeste region.

8. Tanzania: coastal Tanzania and a portion of the coast of southern Kenya.

We exclude regions with less than 2 mm/day in annual-mean rainfall such as the coast of the Horn of Africa and parts of the Middle East, as well as a few islands in the Maritime Continent and Caribbean. Figure 2 shows the mean annual cycle for each of the eight regions listed, averaged over the areas in Figure 1 that receive half or more of their annual rainfall in autumn and winter. The annual cycle of precipitation in these regions displays a remarkably similar pattern consisting of a large peak in rainfall during late autumn or early winter (October-December for the Northern Hemisphere and March-April for the Southern Hemisphere), with a smaller peak during late spring or early summer that may be associated with rainfall received during the summer monsoon in adjacent regions. The large rainfall peak that occurs in these regions during late autumn and early winter, which we will refer to as the autumn monsoon, is the subject of this study. We use the term “autumn monsoon” both in order to highlight the similar timing of the annual peak in precipitation across all of these regions, and to avoid confusion with the anticyclonic winter circulation over East Asia, often referred to as the Asian winter monsoon, which attains its maximum strength between December and February.

Figure 3 shows the climatological rainfall over ocean and land from TRMM during October-December in the Northern Hemisphere and April-June in the Southern Hemisphere, with the gray contour encompassing regions that receive more than half their annual precipitation in autumn and winter, and stippling indicating other regions. Over the global tropics, most rainfall during these months occurs over the ocean, with only a relatively small land area receiving rainfall. Figure 3 also highlights the coastal nature of many of the autumn monsoon regions and their proximity to areas of high precipitation over the ocean. A few other eastern coastal regions, such as southeastern Papua New Guinea and the eastern coast of Madagascar, also receive substantial

amounts of rainfall during this season, but not enough to comprise more than 50% of the year's total rainfall.

In Figure 4, the climatological month of maximum precipitation, after a 5-month running mean is applied, is shown based on CHIRPS data. An interesting feature is the relative scarcity of regions with a spring peak (shown in shades of red-orange in the Northern Hemisphere and violet in the Southern Hemisphere) compared with regions that receive their peak rainfall in autumn (violet in the Northern Hemisphere, red-orange in the Southern Hemisphere). Further, the few regions with a spring peak that do exist do not align systematically with eastern coastlines, unlike regions with an autumn peak. Despite the similar insolation received and the prevailing easterly wind direction in these seasons, an asymmetry exists over the global tropics between spring and autumn that favors precipitation along eastern coastlines during autumn. The origin of this asymmetry is a key question that will be explored in later sections of this paper.

A prominent feature in Figure 4 is the meridional migration of the ITCZ over the continents of Africa and South America. From south to north on these continents, the month of maximum precipitation progresses through the calendar year from austral summer (shades of blue) to boreal summer (shades of orange-yellow), reflecting the migration of the ITCZ from the austral to boreal summer monsoon regions, which cover most of the map. The broad zonal strips over equatorial Africa and South America with peaks in the equinoctial seasons are a consequence of this migration. These regions experience two peaks in their annual cycle that are of near equal magnitude (Wang 1994), unlike the autumn monsoon regions shown in Figure 2.

The delayed peak in rainfall, as well as the location of many of the autumn monsoon regions equatorward of the summer monsoon regions, point to the possibility that they receive their peak rainfall in autumn due to the movement of the ITCZ over these areas. This hypothesis has been advanced in studies of two of these regions: Northeastern Brazil (e.g., Nobre and Shukla 1996;

Hastenrath 2012) and southeastern India (Gadgil 2018). In Section 4, we explore the timing of the ITCZ’s seasonal meridional movement as a possible explanation for the autumn peak in precipitation at these locations.

4. Seasonal Cycle of the ITCZ and Winds

On monthly timescales, the ITCZ lags the latitude of maximum insolation (Waliser and Gautier 1993; Hu et al. 2007), meaning that in many parts of the globe, it is at its most poleward position towards the end of local summer, rather than during the solstices. The offset in the timing of peak rainfall between summer and autumn monsoon regions could thus arise from movement of the ITCZ: as the summer monsoon ends, the ITCZ and the latitude of maximum precipitation shift equatorward in autumn.

Figure 5 shows the movement of the ITCZ over spring and fall. The percentiles of outgoing longwave radiation (OLR) with respect to the distribution of OLR over the tropics (20°S - 20°N) are shown for November and May, with the lowest percentiles indicating the main centers of deep convective activity in those months. The ITCZ location, represented by the latitude of minimum OLR at each longitude, is depicted as a colored line for each autumn month in each hemisphere. These lines, which cross the regions of convective activity, illustrate the migration of the ITCZ away from the poles over the course of autumn.

Nearly all of the autumn monsoon regions do not lie directly beneath the ITCZ during their rainy season: instead, they lie poleward of the main ITCZ at this time of year. Partial exceptions to this general pattern are the Tanzanian coast, over which the ITCZ passes during austral autumn; the Malay Peninsula, which lies beneath the ITCZ in early boreal autumn but not during the months of peak precipitation; and the northern, but not eastern, portion of the Brazilian region. In the

case of Brazil, the passage of the ITCZ through only the northern part of the region suggests that while the northern area is affected by the ITCZ location, the autumn rainfall over the strip of land along the eastern coast, which extends far south of the ITCZ, is governed by other factors. A narrow poleward protrusion of the precipitation contours (shown in white) extends over each of the autumn monsoon regions during the months shown. Robertson et al. (2011) described this phenomenon over the Maritime Continent as a northward extension of the southern summer monsoon; here we note that this feature is not unique to that region and can be seen over multiple continents.

Figure 5, therefore, indicates that meridional movement of the ITCZ over autumn does not explain the autumn rainfall maximum seen in these regions. The ITCZ instead lies equatorward of these regions during the local autumn precipitation peak.

Another significant change that occurs during this time of year in the tropics is the shift in wind direction that accompanies the end of the summer monsoons. During summer, when the ITCZ over land is far from the equator, most monsoon regions experience westerly, poleward winds. As the ITCZ shifts equatorwards, surface winds revert to the easterly, equatorward direction that they display during most of the year. During autumn, therefore, these regions experience northeasterlies and southeasterlies in the Northern and Southern Hemispheres respectively.

Since the peak annual precipitation in the autumn monsoon regions does not occur at the time of year when the large-scale ITCZ passes over them, and because they lie eastward of mountain ranges during periods of easterly winds, we next investigate the possible role of orographic forcing in producing the rainfall peak.

5. An Estimate of the Orographic Contribution to Autumn Monsoon Precipitation

Figure 6 depicts winds 10 m above the surface during autumn in each Hemisphere, along with the topography. As expected, winds are easterly over most of the tropics, including all eight of the autumn monsoon regions. The alignment of the poleward extensions of the rain band seen in Figure 5 with eastern coastlines and their placement on the eastern edges of topographic features (see Figure 6) suggest that the prevailing easterly winds, carrying moist air from tropical oceans, are forced to ascend by orography, producing condensation and precipitation on the windward side of these mountain ranges. Prior work on several of these regions has identified this as a key factor in producing rainfall (e.g., Chang et al. 2016; Lyra et al. 2014; Camberlin and Planchon 1997). This possibility is further supported by the spatial pattern of autumn precipitation in Figure 3, where it can be seen that many autumn monsoon regions are aligned with a nearby mountain range. Since the autumn monsoon regions lie to the east of topographic features, orographic effects may also be responsible for the lack of precipitation received in these regions during summer when they lie on the lee of mountains in low-level westerlies associated with nearby summer monsoons.

We now estimate the rainfall that could be generated by upslope ascent forced by orography and compare the results with observed climatological precipitation in order to assess the importance of this mechanism in producing the autumn rainfall peak.

A few simple models have been proposed for estimating the rainfall produced by orographic forcing (Rhea and Grant 1974; Smith 1979; Alpert and Shafir 1989; Sinclair 1994; Roe 2005). These models assume that air parcels rise parallel to the sloping surface as winds impinge upon the side of a mountain range; therefore, the precipitation produced is proportional to the wind speed in the direction normal to the mountain range, the slope of Earth's surface, and the moisture in the air parcels that are lifted in the upslope flow. While the different models vary in how they account

for the amount of moisture involved in producing precipitation, this proportionality is central to all of them (Smith 2018). We use the model formulated by Smith (1979) and Roe (2005), which was argued to broadly capture climatological patterns of precipitation over spatial scales larger than a few kilometers. This model assumes that condensation removes any supersaturation in rising parcels, and that ascent at every vertical level is equal to the near-surface value set by laminar, convectively stable upslope flow. The latter assumption neglects mountain wave dynamics, but the vertical wavelengths of any such waves may be sufficiently long, relative to the water vapor scale height, to render this an acceptable approximation (see discussion by Kirshbaum et al. 2018). The model rain rate r is then

$$r = \rho_0 q_0 (\mathbf{u}_0 \cdot \nabla z_s) \quad (1)$$

where ρ_0 is the surface air density, q_0 is the specific humidity of surface air (assumed equal to the specific humidity and thus the saturation specific humidity at the lifted condensation level), \mathbf{u}_0 is the horizontal surface wind velocity, and z_s is surface elevation.

Roe (2005) further approximates the saturation humidity of surface air in terms of the sea level value of that quantity and a water vapor scale height, but we do not take that step. By assuming that all condensed moisture falls as precipitation on the windward side of the orography, Equation (1) assumes a precipitation efficiency of unity and neglects microphysical delays. In this sense it constitutes an upper bound on the rainfall produced by upslope flow, but it does not account for the possibility of additional rainfall generated by convection that may be triggered by orographic lifting. While convective activity is to be expected in the tropical regions of interest, the objective of this section is to isolate the contribution of stable upslope flow to the autumn rainfall in order to compare it with the role of moist convection, which is examined in Sections 6 and 7.

Figure 7 displays the seasonal mean rain rates estimated using Equation (1) for each of the regions in autumn. For comparison, the autumn seasonal mean precipitation from observations is also

shown for each region. In all cases, the model predicts some rainfall in the vicinity of the autumn monsoon regions (demarcated by the red contour), but substantially underestimates seasonal-mean precipitation over a large area in each region. It only predicts large rain rates in grid cells immediately adjacent to the mountain ranges, which in many cases (Central America, Venezuela, Philippines, Tanzania) lie further inland than the coastal region that experiences an autumn maximum in precipitation. That deficiency could be remedied by smoothing the distribution of z_s used in the model to crudely represent upstream blocking, but there are other problems with the model's results. In regions such as South Asia, the Malay Peninsula, and northern Brazil, the model predicts very little rainfall in autumn. When averaged spatially within the contour for each region, the predicted rainfall amount is much lower than observed in most cases, with only the estimate in Vietnam being realistic.

In Figure 8, we examine the model's predicted climatological annual cycle of precipitation over land in the autumn monsoon regions, along with each of the contributing factors: wind speed perpendicular to the orographic slope (i.e., $(\mathbf{u}_0 \cdot \nabla z_s)/|\nabla z_s|$) and surface humidity (q_0). When compared with Figure 2, it is clear that this model of orographic rainfall, in addition to underestimating the rainfall amount, fails to describe the seasonal cycle of rainfall. The month of peak rainfall is only accurately predicted in the Philippines and nearly predicted in Vietnam: in most cases, the peak rainfall is predicted to be not in autumn but in winter or early spring, and in the Central American region, a summer peak is predicted. Inspection of the input variables reveals that the large winter peaks arise primarily from the component of the wind velocity normal to the orography. These winter peaks in easterly, equatorward wind speeds represent the lower branch of the winter Hadley Cell. Although the near-surface specific humidity falls rapidly during winter, this change is not large enough to prevent the model from predicting a winter peak in precipitation. While this suggests that the model might perhaps make a more accurate prediction if the specific

humidity were accounted for differently, an examination of the seasonal cycle of specific humidity in these regions indicates otherwise: four of the regions (South Asia, Vietnam, Philippines, and Malaysia) show a peak in surface specific humidity during spring that is larger than that in autumn, meaning that if the dependence on surface specific humidity were amplified the timing of the rainfall peak would still be incorrect. This further raises the question of why, when the surface specific humidity is high and the wind direction is favorable, a large precipitation rate does not occur in these regions during spring.

These results indicate that while a model of convectively stable upslope flow can roughly explain the spatial pattern of autumn monsoon rainfall, this simple model does not explain the quantity of autumn rainfall or the timing of the rainfall peak. It is perhaps not surprising that a model of stable upslope flow would inaccurately describe orographic precipitation in the tropics, where deep moist convection can be influenced strongly by orography (e.g., Smith 1979). Such orographic influence has been studied mostly in summer months (e.g., Medina et al. 2010), but it is clear that even mountain ranges only 1-2 km high can produce strong seasonal-mean precipitation maxima (Grossman and Durran 1984; Xie et al. 2006) by altering pre-existing disturbances (Houze 2012) and, perhaps, by convectively destabilizing the atmosphere (Kirshbaum et al. 2018). The systematic underestimation of rainfall by the above model of stable upslope flow, in spite of the assumed perfect precipitation efficiency, implies that ascent and thus horizontal moisture convergence are amplified by other processes.

We show in the following section that this amplification occurs above the orography with vertical structures suggestive of a role played by moist convection.

6. Moisture Budgets

We calculate moisture budgets for each autumn monsoon region by applying the methodology of Seager and Henderson (2013) to climatological monthly mean data from ERA5. The vertically integrated moisture convergence (VIMC) should equal the difference between precipitation (P) and evaporation (E), i.e.:

$$P - E = -\frac{1}{\rho_w g} \nabla \cdot \int_0^{p_s} \mathbf{u} q \, dp \quad (2)$$

where ρ_w is the density of liquid water, g is the acceleration due to gravity, \mathbf{u} is the wind velocity along pressure surfaces, q is the specific humidity, p is pressure and the subscript s denotes the surface value. The transient storage term is assumed to be negligible on monthly and seasonal timescales. Although reanalyses do not have closed moisture budgets due to assimilation tendencies, we begin by comparing climatological precipitation in each autumn monsoon region from ERA5 with that estimated from TRMM (Figure 9). In all cases, ERA5 reproduces the timing and quantity of precipitation well, with the possible exception of the Philippines, where the annual peak in rainfall is slightly underestimated. The climatologies of surface evaporation and VIMC provided in ERA5, with monthly means of the latter obtained from hourly data, are also shown. The seasonal cycle of VIMC closely resembles that of precipitation, as the evaporation term varies little over the year and is comparatively small. The VIMC computed from climatological monthly mean winds and humidities nearly perfectly reproduces that provided in the reanalysis, confirming that moisture convergence by submonthly transients may be neglected when analyzing the annual cycle of precipitation in these regions. This is consistent with the relatively low contribution of extreme events to the seasonal total precipitation (see Supplemental Materials).

The right-hand side of Equation (2) is then decomposed:

$$-\frac{1}{\rho_w g} \nabla \cdot \int_0^{p_s} \mathbf{u} q \, dp = -\frac{1}{\rho_w g} \int_0^{p_s} q \nabla \cdot \mathbf{u} \, dp - \frac{1}{\rho_w g} \int_0^{p_s} \mathbf{u} \cdot \nabla q \, dp - \frac{1}{\rho_w g} q_s u_s \cdot \nabla p_s \quad (3)$$

On the right-hand side of this equation, the first term represents the component of VIMC that arises due to the convergence of winds (referred to henceforth as the convergence term), the second term represents the component due to horizontal moisture advection (the advection term), and the final term represents the contribution from flow along surface pressure gradients (the surface term). Physically, the surface term includes moisture convergence produced by stable upslope flow, and can be converted into the upslope flow model of Section 5 by using hydrostatic balance to transform from pressure to height coordinates.

Figure 10 displays the annual cycle of these terms in each region. The annual peak in the convergence term in all cases coincides with or is within a month of the annual peak in ERA5 rainfall, indicating its importance in determining the annual cycle of precipitation in these regions. In two of the regions – Vietnam and the Philippines – the surface term also makes a significant contribution, consistent with the prediction of the upslope flow model in the previous section. An additional feature that all of the regions have in common is that the advection term is negative during autumn, indicating that these regions lie downstream of climatologically drier areas.

The convergence term is influenced by the wind divergence and by the humidity, both of which are typically related to convective activity. This, however, does not provide a causal explanation of the seasonal cycle, as the increase in the convergence term may arise from changes in the wind field or in humidity. To identify the contributions of these factors, we perform a Reynolds decomposition of the moisture convergence,

$$\nabla \cdot \langle \mathbf{u}q \rangle = \nabla \cdot \langle \bar{\mathbf{u}}\bar{q} \rangle + \nabla \cdot \langle \mathbf{u}'\bar{q} \rangle + \nabla \cdot \langle \bar{\mathbf{u}}q' \rangle + \nabla \cdot \langle \mathbf{u}'q' \rangle \quad (4)$$

where for the quantity x , $\langle x \rangle$ denotes $-\frac{1}{\rho_w g} \int_0^{p_s} x dp$, \bar{x} is its annual mean, and x' is the deviation of the climatological monthly mean from the annual mean. The monthly mean values of each term during the month of maximum climatological precipitation are shown for the autumn monsoon

regions in Table 2. In all cases, the seasonal variation in moisture convergence is dominated by the term containing the deviation of velocity from its annual mean, i.e., $\nabla \cdot \langle \mathbf{u}' \bar{q} \rangle$. This indicates that it is not anomalous moisture in relatively steady flow that is responsible for the autumn peak in rainfall, but that changes in the divergent wind field (i.e. ascent) primarily control the timing of rainfall. The analysis of Section 5 showed that ascent induced by stable upslope flow was not sufficient to explain the observed autumn rainfall, suggesting a role for convectively coupled ascent. In the following section, we examine the vertical motion in these regions and the large-scale forcings that may induce it.

7. Factors Influencing Moist Convection

Figure 11 displays the annual cycles of vertical mass flux (colors) and relative humidity (contours) of the atmospheric column averaged over each of the autumn monsoon regions (the mass flux is the ERA5 pressure-coordinate vertical velocity divided by g). In all eight regions, there is ascent and high relative humidity throughout the column during the months of peak rainfall, suggesting the presence of deep convection. This vertical mass flux is associated with the convergence term of Equation (3) and the monthly variations of the wind field, i.e., $\nabla \cdot \langle \mathbf{u}' \bar{q} \rangle$ in Equation (4), which dominate the annual cycle. In many cases, peak ascent during the rainy season occurs in the lower troposphere, below approximately 700 hPa. Exceptions to this typical profile are found in the Indo-Pacific's Malay Peninsula and South Asia, where the vertical mass flux peaks near 300 hPa – characteristic of the broader Indo-Pacific Warm Pool region. Peak ascent over the Venezuelan region is in the mid-troposphere near 500 hPa.

As seen in previous sections, ascent in all regions has a seasonal cycle and autumn magnitude that cannot be explained primarily by stable upslope ascent of the Trade winds (e.g. Figure 8 and the

surface term in Figure 10). The observed autumn ascent must be stronger and, in some regions (South Asia, the Malay Peninsula, and Venezuela), more top-heavy than one would expect from such an upslope flow model. Two partial exceptions to this are Vietnam and the Philippines, where very bottom-heavy ascent (Figure 11 d, f) is consistent with the surface term both accounting for a large fraction of autumn rainfall and having a high-amplitude seasonal cycle in phase with the autumn peak (Figure 10 d, f). Nevertheless, even in Vietnam and the Philippines, the total moisture convergence in the autumn peak is roughly twice that contributed by the surface term. The central question is thus what drives the magnitude and seasonal cycle of ascent seen in Figure 11.

A prominent feature of Figure 11 is the large differences in ascent between the autumn rainy season and early spring/late winter, with both relative humidity and ascent near their annual minimum through much of the column in the latter period. The asymmetry in rainfall between spring and autumn has been previously studied in the Maritime Continent (Hung et al. 2004; Chang et al. 2005; Wang and Chang 2008; Robertson et al. 2011). Chang et al. (2005) hypothesized that this asymmetry may occur due to the high heat capacity of the ocean: after peak insolation is received in summer, the ocean retains the energy received for a few months, causing the sea surface to be on average warmer in autumn than in spring. Due to the low heat capacity of the land surface, the continents poleward of the Maritime Continent warm more rapidly than the ocean in spring and cool more rapidly in autumn, giving rise to a meridional pressure gradient in autumn that results in more precipitation over the Maritime Continent. In a subsequent study, Wang and Chang (2008) tested this hypothesis using imposed SSTs in a general circulation model and were able to reproduce features of the observed spatial pattern of precipitation in these seasons in the Maritime Continent. At a more global scale, it has long been noted that the mean latitude of the ITCZ lags that of maximum insolation (e.g., Waliser and Gautier 1993; Hu et al. 2007). This lag has been explained using similar arguments in idealized models: warmer SSTs in autumn than in

spring, due to the ocean's high heat capacity, cause the ITCZ to remain in the autumn hemisphere until the onset of the summer monsoon in the other hemisphere (Xian and Miller 2008; Wei and Bordoni 2018). While the analysis in Section 4 shows that the autumn monsoon regions do not lie directly beneath the main ITCZ, this is a possible explanation for why convection is favored in these regions in autumn: SSTs peak in these regions at that time of year.

To assess whether this mechanism operates over autumn monsoon regions, we examine the seasonal cycle of SSTs in these regions (Figure 12). While the months of maximum SST do occur in autumn in some of these locations (those in the Atlantic sector and Tanzania), the mechanism outlined above cannot provide an explanation for half of the cases, particularly in the Indo-Pacific, where maximum local SSTs occur in spring rather than autumn. This suggests that local surface temperatures alone do not determine the occurrence of the precipitating ascent that produces autumn rainfall. The seasonal cycle of near-surface humidity over land strongly resembles that of local SSTs (compare with Figure 8), indicating that this behavior is not confined to ocean regions alone: the months of peak near-surface humidity over land are not the months of peak rainfall.

Recognizing that low-latitude ascent is not controlled by local SST alone, we assess the favorability of large-scale conditions for deep convection by examining the relative SST (RSST), calculated as the difference between local SST and SST spatially-averaged over the global tropics (20°S - 20°N). The underlying argument for using RSST is that the temperature of the upper troposphere in the tropics, which is relatively spatially uniform (Sobel and Bretherton 2000), is set by the spatially averaged SST (Sobel et al. 2002) on timescales longer than approximately one month. Therefore, for conditions to facilitate convection at a given location, the SST at that location must be warm relative to that of other tropical regions, i.e., the RSST must be positive to reduce the stability of the column. RSST has proven useful in a range of contexts as an indicator of the large-scale forcing for deep convection, including in assessing the effects of anthropogenic climate change (Johnson

and Xie 2010), characterizing ENSO variability (Williams and Patricola 2018), and estimating the probability of tropical cyclone formation (Vecchi and Soden 2007; Ramsay and Sobel 2011).

Izumo et al. (2020) demonstrated the effectiveness of RSST in predicting the spatial pattern of tropical oceanic rainfall using monthly-mean data. Unlike convective available potential energy (CAPE), which is rapidly consumed by convective activity and therefore not a reliable indicator of the conditions promoting or suppressing convection over timescales longer than a few days, RSST remains comparatively stable over monthly timescales, providing a useful proxy for the influence of surface forcings and free-tropospheric temperature on the annual cycle of moist convection.

Figure 12 shows that RSST peaks in the season of maximum rainfall and maximum ascent in each region, with the exception of the Philippines. In the Philippines, the maximum RSST occurs in local summer, when the wind direction is such that this autumn monsoon region lies on the lee of nearby mountains; this is consistent with upslope winds and the surface term making a larger contribution to the seasonal cycle of rainfall there. In all other cases, however, the RSST is highest in autumn, indicating that this is the season most favorable for moist convection in these regions.

While the timing of peaks and troughs of RSST is similar to that of SST in some regions (those in the Atlantic sector and Tanzania), in the Indo-Pacific sector, the shape of the RSST curve differs substantially from that of the SST curve, with RSST and SST peaks occurring nearly six months apart. To understand this discrepancy between the annual cycles of RSST and SST, we examine the seasonal cycle of tropical mean SST (i.e., the term subtracted from the local SST to arrive at the RSST) in Figure 13.

Tropical-mean SST peaks in boreal spring, with substantially cooler temperatures in boreal autumn. Local SSTs thus need to be higher during boreal spring to force convection than during the rest of the year. In the autumn monsoon regions in the vicinity of the Warm Pool, SST variations over the course of the year are small (Figure 12). Peak SSTs during boreal spring in

these regions are not warm enough to facilitate convection during the months of the year with the highest tropical mean SST; however, during autumn when the tropical-mean SST is lower, local SSTs are sufficient to enable convection. In contrast, in the Northern Hemisphere regions in the Atlantic sector and in the Southern Hemisphere regions, RSST and SST both peak during local autumn, i.e., the amplitude of the seasonal cycle of local SSTs is large enough that subtracting the tropical-mean SST does not produce a change in the timing of the peak RSST.

We further investigate the seasonal cycle of tropical-mean SST in Panel (b) of Figure 13, which shows the difference in seasonal mean SST between spring and autumn. Blue regions indicate cooler SSTs in boreal autumn, and orange regions indicate warmer SSTs in boreal autumn. The largest absolute values, reaching 4–5°C, are found over the eastern cold tongues in the equatorial Pacific and Atlantic Oceans. These features, which are characterized by upwelling at the equator and eastern boundaries of ocean basins, exist due to Ekman pumping induced by prevailing easterly winds. The seasonal cycle of the oceanic ITCZ subjects large swaths of the tropical oceans to southeasterly winds in boreal autumn, intensifying the upwelling of cool subsurface waters that occurs throughout the year; northeasterlies in boreal spring suppress this upwelling and raise SSTs (Li and Philander 1996, 1997). We hypothesize that these large upwelling zones therefore stabilize the zonal-mean troposphere in boreal spring, explaining the lack of a phenomenon similar to the autumn monsoon in spring in the Northern Hemisphere. A related hypothesis was outlined in Wang (1994) to explain the drier boreal spring than autumn months in the Maritime Continent region: cooler SSTs over the eastern equatorial Pacific intensify the zonal SST gradient across the Indo-Pacific during boreal autumn, thereby strengthening the Walker circulation and enhancing convection in the region during these months compared to boreal spring. The mechanism we propose applies more broadly to the entire tropics, with the most pronounced effect on the Indo-Pacific where the amplitude of the annual cycle of SSTs is small.

The RSST alone does not, however, provide a complete explanation of the timing of the rainfall peak: although the tropical-mean SST is lowest in August, and many of the regions thus have positive RSST, the westerly wind direction at this time of year places all of the Northern Hemisphere autumn monsoon regions on the lee of mountain ranges. In the Philippines, this effect dominates and upslope flow seems to exert a stronger control on rainfall. There is a smaller offset between the RSST and precipitation peaks over Vietnam which is likely due to the same reason. Therefore, the timing of peak rainfall in these regions depends not only on the local RSST but also on the wind direction with respect to topography.

8. Summary and Discussion

We have identified eight eastern coastal tropical regions on multiple continents that experience their primary rainfall season during local autumn. This sets them apart from most land regions in the tropics, which experience maximum rainfall during summer as part of a local monsoon circulation. Despite the high population density of these coastal areas, the annual cycle of their precipitation has received relatively little attention, and they have not previously been considered as part of a unified global phenomenon. We observe several common features shared by these regions despite their geographic separation:

1. They lie on the eastern margins of landmasses, and are typically narrow.
2. They lie in close proximity to long mountain ranges of modest height.
3. They receive most of their annual rainfall in late autumn, and experience a substantially smaller rainfall peak in late spring or summer.

4. Winds in these regions are easterly and equatorward during the months of maximum precipitation.
5. They do not lie directly beneath the ITCZ during the months of maximum rainfall: the annual peak in rainfall in these locations occurs when the ITCZ is equatorward of them.

Based on these common features, we propose that these regions constitute a particular climate type or regime, underpinned by common dynamics. Analyses in Sections 4 to 7 support this thesis.

In this work, we observe and explain two asymmetries in the annual cycle of observed tropical precipitation. The first asymmetry is spatial: why do tropical regions with their primary season of rainfall in autumn systematically lie along eastern coastlines? This spatial pattern can be attributed to the presence of meridionally oriented mountain ranges that shield these regions from the summer monsoon westerlies and facilitate orographic ascent during other seasons, including autumn, when the prevailing winds are easterly. The second is the temporal asymmetry between autumn and spring: although the prevailing winds are easterly and the surface humidity is high in several of these regions during local spring, they receive significantly less rainfall in spring than in autumn. This, in all cases, is related to the difference in local atmospheric stability at these times of year: we find that conditions are more favorable for moist convection in autumn than in spring, attributable in part to the effect of local SSTs but also to the remote influence of the seasonal cycle of upwelling in the equatorial Pacific and Atlantic oceans.

The use of relative SST as a metric in this context allows us to interpret the effects of the large-scale coupled tropical ocean-atmosphere system on local precipitation. While relative SST-based metrics have been used widely in studying tropical cyclone activity and interannual variability, this is the first use of such a metric, to our knowledge, in understanding the annual cycle of tropical precipitation.

The annual cycle of wind over the equatorial Pacific and Atlantic Oceans in the modern climate is such that equatorial and coastal upwelling in the eastern parts of these basins are both most vigorous and of largest spatial extent during boreal autumn, resulting in large swaths of cool SSTs that reduce the tropical-mean SST. This implies that over the rest of the tropics, this is the most favorable time of year for deep convection: a conclusion further supported by the peak tropical cyclone season in many Northern Hemisphere regions occurring during boreal autumn. Idealized aquaplanet studies examining the asymmetry of tropical precipitation between autumn and spring (Xian and Miller 2008; Wei and Bordoni 2018) have concluded that the asymmetry arises due to the high heat capacity of the ocean, which results in a lag of a few months between the timing of maximum insolation and maximum SST, causing the ITCZ to linger in the autumn hemisphere. However, we find that the highest SSTs in the annual cycle of many autumn monsoon regions occur in spring rather than fall, indicating that factors other than ocean heat capacity, such as ocean dynamics or cloud radiative effects, significantly affect the annual cycle of SSTs. Our results suggest an alternative hypothesis for why more rainfall occurs in boreal autumn than spring, given the modern configuration of continents and insolation, with a key role played by upwelling in the equatorial cold tongue regions of the Pacific and Atlantic basins. This hypothesis is distinct from and more geographically general than that proposed by Chang et al. (2005) for the seasonal cycle in the Maritime Continent, which invoked sea level pressure gradients induced by the differing heat capacities of land and ocean, together with the particular locations and shapes of the Asian and Australian landmasses.

Our hypothesis raises the possibility that the timing of the annual precipitation peak in many autumn monsoon regions may be sensitive to changes in properties of the cold tongue regions. In past climates with a different configuration of continents or orbital forcing, this may have resulted in an altered annual cycle of upwelling (e.g., Bush 1999; Fedorov et al. 2006; Arbuszewski et al.

2013) and therefore of precipitation in many of these regions. This would also imply that under anthropogenic climate change, the precipitation in these regions will depend not only on changes in the seasonal cycle of local SSTs but also on that of the eastern upwelling zones.

Here we showed that several mechanistic arguments are consistent with observations of the climatological seasonal cycle of the atmosphere and ocean; further work is needed to rigorously test these ideas by perturbing relevant processes in idealized and realistic models. Examining the observed interannual variations and historical trends in these autumn monsoon regions may also further advance understanding. Nevertheless, the results presented here demonstrate that factors such as the local SST or the seasonal cycle of wind-orography interaction are insufficient, in isolation, to account for the unusual seasonal cycle observed in autumn monsoon regions. Perhaps more importantly, this work identifies a previously unrecognized climate regime that appears in eastern coastal regions around the globe.

Acknowledgments. This work was supported by the U.S. Department of Energy, Office of Science, Biological and Environmental Research under Award Number DE-SC0019367 and by National Science Foundation Award AGS-1746160. N.R. was partially supported by the Australian Research Council (Data Analytics for Resources and Environments, Grant IC190100031) during the completion of this work.

Data availability statement. The datasets analyzed in this study are publicly available at locations cited in the reference section.

References

- Aceituno, P., M. del Rosario Prieto, M. E. Solari, A. Martínez, G. Poveda, and M. Falvey, 2009: The 1877–1878 el nio episode: associated impacts in south america. *Climatic Change*, **92** (3-4),

389–416.

Aldrian, E., and R. D. Susanto, 2003: Identification of three dominant rainfall regions within indonesia and their relationship to sea surface temperature. *International Journal of Climatology: A Journal of the Royal Meteorological Society*, **23** (12), 1435–1452.

Alpert, P., and H. Shafir, 1989: Mesoy-scale distribution of orographic precipitation: Numerical study and comparison with precipitation derived from radar measurements. *Journal of applied meteorology*, **28** (10), 1105–1117.

Amante, C., and B. Eakins, 2009: Etopo1 1 arc-minute global relief model: Procedures, data sources and analysis. *Memorandum NESDIS NGDC-24*.

Aparicio, J., P. F. Martínez-Austria, A. Güitrón, and A. I. Ramírez, 2009: Floods in tabasco, mexico: a diagnosis and proposal for courses of action. *Journal of Flood Risk Management*, **2** (2), 132–138.

Arbuszewski, J. A., P. B. Demenocal, C. Cléroux, L. Bradtmiller, and A. Mix, 2013: Meridional shifts of the atlantic intertropical convergence zone since the last glacial maximum. *Nature Geoscience*, **6** (11), 959–962.

Beck, H. E., N. E. Zimmermann, T. R. McVicar, N. Vergopolan, A. Berg, and E. F. Wood, 2018: Present and future köppen-geiger climate classification maps at 1-km resolution. *Scientific Data*, **5** (1), doi:10.1038/sdata.2018.214, URL <https://doi.org/10.1038/sdata.2018.214>.

Bush, A. B., 1999: Assessing the impact of mid-holocene insolation on the atmosphere-ocean system. *Geophysical Research Letters*, **26** (1), 99–102.

Camberlin, P., and O. Planchon, 1997: Coastal precipitation regimes in kenya. *Geografiska Annaler: Series A, Physical Geography*, **79** (1-2), 109–119.

- Chang, C., Z. Wang, J. Ju, and T. Li, 2004: On the relationship between western maritime continent monsoon rainfall and enso during northern winter. *Journal of Climate*, **17** (3), 665–672.
- Chang, C.-P., M.-M. Lu, and H. Lim, 2016: Monsoon convection in the maritime continent: Interaction of large-scale motion and complex terrain. *Meteorological Monographs*, **56**, 6–1.
- Chang, C.-P., Z. Wang, and H. Hendon, 2006: The asian winter monsoon. *The Asian Monsoon*, Springer, 89–127.
- Chang, C.-P., Z. Wang, J. McBride, and C.-H. Liu, 2005: Annual cycle of southeast asia—maritime continent rainfall and the asymmetric monsoon transition. *Journal of climate*, **18** (2), 287–301.
- Chen, T.-C., J.-D. Tsay, M.-C. Yen, and J. Matsumoto, 2012: Interannual variation of the late fall rainfall in central vietnam. *Journal of Climate*, **25** (1), 392–413.
- Chen, T.-C., J.-D. Tsay, M.-C. Yen, and J. Matsumoto, 2013: The winter rainfall of malaysia. *Journal of climate*, **26** (3), 936–958.
- Davis, M., 2002: *Late Victorian holocausts: El Niño famines and the making of the third world*. Verso Books.
- Fedorov, A., P. Dekens, M. McCarthy, A. Ravelo, P. DeMenocal, M. Barreiro, R. Pacanowski, and S. Philander, 2006: The pliocene paradox (mechanisms for a permanent el niño). *Science*, **312** (5779), 1485–1489.
- Funk, C., and Coauthors, 2015: The climate hazards infrared precipitation with stations—a new environmental record for monitoring extremes. *Scientific data*, **2** (1), 1–21.
- Gadgil, S., 2018: The monsoon system: Land–sea breeze or the itcz? *Journal of Earth System Science*, **127** (1), 1.

Gamoyo, M., C. Reason, and D. Obura, 2015: Rainfall variability over the east african coast. *Theoretical and Applied Climatology*, **120** (1-2), 311–322.

Giannini, A., R. Saravanan, and P. Chang, 2004: The preconditioning role of tropical atlantic variability in the development of the enso teleconnection: Implications for the prediction of nordeste rainfall. *Climate Dynamics*, **22** (8), 839–855.

Greenfield, G. M., 2001: The realities of images: imperial brazil and the great drought. *Transactions of the American Philosophical Society*, **91** (1), ii–148.

Grossman, R. L., and D. R. Durran, 1984: Interaction of Low-Level Flow with the Western Ghat Mountains and Offshore Convection in the Summer Monsoon. *Monthly Weather Review*, **112** (4), 652–672, doi:10.1175/1520-0493(1984)112<0652:IOLFW>2.0.CO;2.

Guha-Sapir, D., R. Below, and P. Hoyois, 2016: EM-DAT: The CRED/OFDA international disaster database. Université Catholique de Louvain, <https://www.emdat.be/>.

Hastenrath, S., 2012: Exploring the climate problems of brazil's nordeste: a review. *Climatic Change*, **112** (2), 243–251.

Hastenrath, S., D. Polzin, and C. Mutai, 2011: Circulation mechanisms of kenya rainfall anomalies. *Journal of Climate*, **24** (2), 404–412.

Hersbach, H., and Coauthors, 2020: The era5 global reanalysis. *Quarterly Journal of the Royal Meteorological Society*.

Houze, R. A., Jr, 2012: Orographic effects on precipitating clouds. *Reviews of Geophysics*, **50** (1).

Hu, Y., D. Li, and J. Liu, 2007: Abrupt seasonal variation of the ITCZ and the hadley circulation. *Geophysical Research Letters*, **34** (18), doi:10.1029/2007gl030950.

Huffman, G. J., and Coauthors, 2007: The trmm multisatellite precipitation analysis (tmpa): Quasi-global, multiyear, combined-sensor precipitation estimates at fine scales. *Journal of hydrometeorology*, **8** (1), 38–55.

Hung, C.-w., X. Liu, and M. Yanai, 2004: Symmetry and asymmetry of the asian and australian summer monsoons. *Journal of Climate*, **17** (12), 2413–2426.

Izumo, T., J. Vialard, M. Lengaigne, and I. Suresh, 2020: Relevance of relative sea surface temperature for tropical rainfall interannual variability. *Geophysical Research Letters*, **47** (3), e2019GL086182, doi:10.1029/2019GL086182.

Johnson, N. C., and S.-P. Xie, 2010: Changes in the sea surface temperature threshold for tropical convection. *Nature Geoscience*, **3** (12), 842–845.

Kirshbaum, D. J., B. Adler, N. Kalthoff, C. Barthlott, and S. Serafin, 2018: Moist orographic convection: Physical mechanisms and links to surface-exchange processes. *Atmosphere*, **9** (3), 80.

Kripalani, R., and P. Kumar, 2004: Northeast monsoon rainfall variability over south peninsular india vis-à-vis the indian ocean dipole mode. *International Journal of Climatology: A Journal of the Royal Meteorological Society*, **24** (10), 1267–1282.

Kumar, P., K. R. Kumar, M. Rajeevan, and A. K. Sahai, 2006: On the recent strengthening of the relationship between ENSO and northeast monsoon rainfall over south asia. *Climate Dynamics*, **28** (6), 649–660, doi:10.1007/s00382-006-0210-0.

Kumaran, T. V., O. Murali, and S. R. Senthamarai, 2020: Chennai floods 2005, 2015: Vulnerability, risk and climate change. *Urban Health Risk and Resilience in Asian Cities*, Springer, 73–100.

Li, T., and S. Philander, 1997: On the seasonal cycle of the equatorial atlantic ocean. *Journal of Climate*, **10** (4), 813–817.

Li, T., and S. G. H. Philander, 1996: On the annual cycle of the eastern equatorial pacific. *Journal of Climate*, **9** (12), 2986–2998.

Liebmann, B., and C. A. Smith, 1996: Description of a complete (interpolated) outgoing longwave radiation dataset. *Bulletin of the American Meteorological Society*, **77** (6), 1275–1277.

Lyon, B., 2003: Enhanced seasonal rainfall in northern venezuela and the extreme events of december 1999. *Journal of Climate*, **16** (13), 2302–2306.

Lyon, B., and D. G. DeWitt, 2012: A recent and abrupt decline in the east african long rains. *Geophysical Research Letters*, **39** (2).

Lyra, G. B., J. F. Oliveira-Júnior, and M. Zeri, 2014: Cluster analysis applied to the spatial and temporal variability of monthly rainfall in alagoas state, northeast of brazil. *International Journal of Climatology*, **34** (13), 3546–3558.

Medina, S., R. A. Houze Jr., A. Kumar, and D. Niyogi, 2010: Summer monsoon convection in the himalayan region: terrain and land cover effects. *Quarterly Journal of the Royal Meteorological Society*, **136** (648), 593–616, doi:10.1002/qj.601.

Nobre, P., and J. Shukla, 1996: Variations of sea surface temperature, wind stress, and rainfall over the tropical atlantic and south america. *Journal of Climate*, **9** (10), 2464–2479, doi:10.1175/1520-0442(1996)009<2464:VOSSTW>2.0.CO;2.

Pezzi, L., and I. Cavalcanti, 2001: The relative importance of enso and tropical atlantic sea surface temperature anomalies for seasonal precipitation over south america: a numerical study. *Climate Dynamics*, **17** (2-3), 205–212.

- Portig, W., 1965: Central american rainfall. *Geographical Review*, **55** (1), 68–90.
- Pulwarty, R. S., R. G. Barry, and H. Riehl, 1992: Annual and seasonal patterns of rainfall variability over venezuela (jährliche und jahreszeitliche muster der niederschlagsvariabilität in venezuela). *Erdkunde*, 273–289.
- Ramage, C., J. Marshall, and R. Plumb, 1971: *Monsoon Meteorology*, International Geophysics Series, Vol. 15. Academic Press.
- Ramsay, H. A., and A. H. Sobel, 2011: Effects of relative and absolute sea surface temperature on tropical cyclone potential intensity using a single-column model. *Journal of Climate*, **24** (1), 183–193.
- Reynolds, R. W., N. A. Rayner, T. M. Smith, D. C. Stokes, and W. Wang, 2002: An improved in situ and satellite SST analysis for climate. *Journal of Climate*, **15** (13), 1609–1625, doi: 10.1175/1520-0442(2002)015<1609:aiisas>2.0.co;2.
- Rhea, J. O., and L. Grant, 1974: Topographic influences on snowfall patterns in mountainous terrain. *Advanced Concepts and Techniques in the Study of Snow and Ice Resources*.
- Robertson, A. W., V. Moron, J.-H. Qian, C.-P. Chang, F. Tangang, E. Aldrian, T. Y. Koh, and J. Liew, 2011: The maritime continent monsoon. *The global monsoon system: research and forecast*, World Scientific, 85–98.
- Roe, G. H., 2005: Orographic precipitation. *Annual Review of earth and planetary sciences*, **33** (1), 645–671.
- Seager, R., and N. Henderson, 2013: Diagnostic computation of moisture budgets in the era-interim reanalysis with reference to analysis of cmip-archived atmospheric model data. *Journal of Climate*, **26** (20), 7876–7901.

- Sinclair, M. R., 1994: A diagnostic model for estimating orographic precipitation. *Journal of applied meteorology*, **33** (10), 1163–1175.
- Singh, N., and N. Sontakke, 1999: On the variability and prediction of post-monsoon rainfall over india. *Int. J. Climatol.*, **19**, 309–39.
- Smith, R. B., 1979: The influence of mountains on the atmosphere. *Advances in geophysics*, **21**, 87–230.
- Smith, R. B., 2018: 100 years of progress on mountain meteorology research. *Meteorological Monographs*, **59**, 20–1.
- Sobel, A. H., and C. S. Bretherton, 2000: Modeling tropical precipitation in a single column. *Journal of climate*, **13** (24), 4378–4392.
- Sobel, A. H., I. M. Held, and C. S. Bretherton, 2002: The enso signal in tropical tropospheric temperature. *Journal of climate*, **15** (18), 2702–2706.
- Suppiah, R., 1989: Relationships between the southern oscillation and the rainfall of sri lanka. *International Journal of Climatology*, **9** (6), 601–618.
- Trewartha, G. T., 1961: *The earth's problem climates*. University of Wisconsin Press.
- Uvo, C. B., C. A. Repelli, S. E. Zebiak, and Y. Kushnir, 1998: The relationships between tropical pacific and atlantic sst and northeast brazil monthly precipitation. *Journal of Climate*, **11** (4), 551–562.
- van Oldenborgh, G. J., F. E. Otto, K. Haustein, and K. AchutaRao, 2016: The heavy precipitation event of december 2015 in chennai, india. *Bulletin of the American Meteorological Society*, **97** (12), S87–S91.

- Vecchi, G. A., and B. J. Soden, 2007: Effect of remote sea surface temperature change on tropical cyclone potential intensity. *Nature*, **450** (7172), 1066–1070.
- Waliser, D. E., and C. Gautier, 1993: A satellite-derived climatology of the itcz. *Journal of climate*, **6** (11), 2162–2174.
- Wang, B., 1994: Climatic regimes of tropical convection and rainfall. *Journal of Climate*, **7** (7), 1109–1118.
- Wang, Z., and C. Chang, 2008: Mechanism of the asymmetric monsoon transition as simulated in an agcm. *Journal of climate*, **21** (8), 1829–1836.
- Wei, H.-H., and S. Bordoni, 2018: Energetic constraints on the itcz position in idealized simulations with a seasonal cycle. *Journal of Advances in Modeling Earth Systems*, **10** (7), 1708–1725.
- Williams, I. N., and C. M. Patricola, 2018: Diversity of enso events unified by convective threshold sea surface temperature: a nonlinear enso index. *Geophysical Research Letters*, **45** (17), 9236–9244.
- Xian, P., and R. L. Miller, 2008: Abrupt seasonal migration of the ITCZ into the summer hemisphere. *Journal of the Atmospheric Sciences*, **65** (6), 1878–1895, doi:10.1175/2007jas2367.1.
- Xie, S.-P., H. Xu, N. Saji, Y. Wang, and W. T. Liu, 2006: Role of narrow mountains in large-scale organization of asian monsoon convection. *Journal of climate*, **19** (14), 3420–3429.
- Yadav, R. K., 2013: Emerging role of indian ocean on indian northeast monsoon. *Climate dynamics*, **41** (1), 105–116.
- Yang, W., R. Seager, M. A. Cane, and B. Lyon, 2015: The annual cycle of east african precipitation. *Journal of Climate*, **28** (6), 2385–2404.

- Yokoi, S., and J. Matsumoto, 2008: Collaborative effects of cold surge and tropical depression-type disturbance on heavy rainfall in central vietnam. *Monthly Weather Review*, **136** (9), 3275–3287.
- Zhang, S., and B. Wang, 2008: Global summer monsoon rainy seasons. *International Journal of Climatology*, **28** (12), 1563–1578, doi:10.1002/joc.1659.
- Zubair, L., 2002: El nino–southern oscillation influences on rice production in sri lanka. *International Journal of Climatology*, **22** (2), 249–260.
- Zubair, L., S. A. Rao, and T. Yamagata, 2003: Modulation of sri lankan maha rainfall by the indian ocean dipole. *Geophysical Research Letters*, **30** (2).

LIST OF TABLES

Table 1. The data sets used in this study.	39
Table 2. The climatological monthly mean values of each of the terms in the Reynolds decomposition of the moisture convergence (Equation 4) during the climatological month of maximum precipitation (based on ERA5) in each autumn monsoon region in units of mm/day. Note that positive values indicate convergence (see text).	40

TABLE 1. The data sets used in this study.

	Data set	Variables Used	Spatial Resolution (degrees)	Vertical levels	Coverage	Time period	Reference
1.	Climate Hazards center InfraRed Precipitation with Station data (CHIRPS)	Precipitation	0.05	Surface	Land only	1981-2019	Funk et al. (2015)
2.	Tropical Rainfall Measuring Mission Multi-satellite Precipitation Analysis 3B43 (TRMM)	Precipitation	0.25	Surface	Land and ocean	1998-2019	Huffman et al. (2007)
3.	European Center for Medium-Range Weather Forecasts Re-analysis 5th Generation (ERA5)	Precipitation, vertical and horizontal velocity, specific humidity, relative humidity, moisture convergence, convective available potential energy (CAPE)	0.25	37 levels	Land and ocean	1979-2013	Hersbach et al. (2020)
4.	ETOPO1 1 Arc-Minute Global Relief Model (ETOPO)	Surface height	0.02	-	Land and ocean		Amante and Eakins (2009)
5.	National Oceanic and Atmospheric Administration Optimum Interpolation Sea Surface Temperature v2.0 (OISST)	Sea surface temperature	1	Surface	Ocean only	1982-2019	Reynolds et al. (2002)
6.	National Oceanic and Atmospheric Administration Interpolated Outgoing Longwave Radiation (NOAA-OLR)	Outgoing Longwave Radiation (OLR)	2.5	Top of Atmosphere	Land and ocean	1975-2019	Liebmann and Smith (1996)

TABLE 2. The climatological monthly mean values of each of the terms in the Reynolds decomposition of the moisture convergence (Equation 4) during the climatological month of maximum precipitation (based on ERA5) in each autumn monsoon region in units of mm/day. Note that positive values indicate convergence (see text).

	Region	Month	$\nabla \cdot \langle \mathbf{u}q \rangle - \nabla \cdot \langle \bar{\mathbf{u}}\bar{q} \rangle$	$\nabla \cdot \langle \mathbf{u}'\bar{q} \rangle$	$\nabla \cdot \langle \bar{\mathbf{u}}q' \rangle$	$\nabla \cdot \langle \mathbf{u}'q' \rangle$
1.	Central America	October	5.24	4.9	-0.08	0.42
2.	Venezuela	October	3.66	4.15	-0.63	0.14
3.	South Asia	November	4.40	4.27	-0.28	0.41
4.	Malay Peninsula	November	4.59	4.33	0.17	0.09
5.	Vietnam	October	3.44	3.30	0.13	0.02
6.	Philippines	November	2.52	2.50	0.06	-0.03
7.	Brazil	April	5.41	4.54	0.39	0.48
8.	Tanzania	April	2.14	2.52	-0.33	-0.06

LIST OF FIGURES

- Fig. 1.** The climatological fraction of annual rainfall that occurs during the fall and winter months in (a) the Northern Hemisphere (September to February) and (b) the Southern Hemisphere (March to August). Shades of red and orange indicate regions where half or more of the annual rainfall occurs during these months. Gray boxes highlight the eight regions examined in this study, numbered as in the text of Section 3. 43

Fig. 2. The climatological annual cycle of precipitation (mm/day) averaged over the areas that receive more than half of their annual rainfall in local autumn and winter in (a) the Northern Hemisphere and (b) the Southern Hemisphere. Spatial averaging was performed over the land areas within the boxes indicated in Figure 1 using CHIRPS data with locations receiving less than half of their annual rainfall in autumn and winter excluded. 44

Fig. 3. The climatological precipitation (mm/day) averaged over late autumn and early winter in each hemisphere (October to December in (a) and April to June in (b)) from TRMM. The gray contour demarcates areas that receive more than half of their annual rainfall in local autumn and winter (September to February in (a) and March to August in (b)); regions that receive more than half of their annual rainfall during spring and summer are stippled. Light gray boxes indicate the regions used for averaging in Sections 6 and 7. 44

Fig. 4. The climatological month of maximum precipitation at each location from CHIRPS, after a 5-month running mean was applied to the annual cycle. Regions with annual-mean rainfall less than 2 mm/day are indicated in gray. 46

Fig. 5. The percentile of outgoing longwave radiation (OLR) with respect to the climatological distribution of OLR over the tropics in (a) November and (b) May (colors). An uneven color scale is used to highlight the lower percentiles, which suggest convective activity. Contours of 5 mm/day and 15 mm/day of climatological precipitation are shown for the corresponding months in white. Colored lines in panels (a) and (b) indicate the latitude of minimum OLR within the tropics during boreal and austral autumn respectively (see legend), with bold orange lines representing the month for which the other variables in each panel are shown. The latitude of minimum OLR has been smoothed for visualization using a Parzen filter with a window of 7.5° . Green boxes highlight the eight autumn monsoon regions. 47

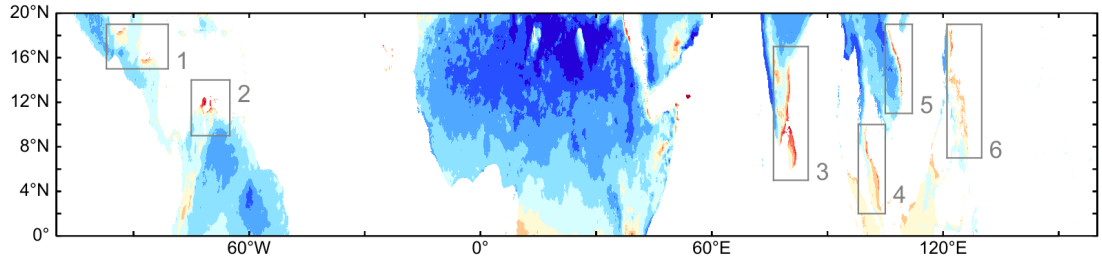
Fig. 6. The height of the land surface above sea level (colors) and the climatological seasonal mean wind field at 10 m above the surface (arrows) in (a) October to December in the Northern Hemisphere and (b) April to June in the Southern Hemisphere. 48

Fig. 7. The climatological precipitation predicted by the orographic model (1st and 3rd columns) and from TRMM (2nd and 4th columns) for comparison in each region, averaged over October–December in the Northern Hemisphere (a-l) and April–June in the Southern Hemisphere (m-p). The red contour demarcates the regions that receive more than half of their annual rainfall in autumn and winter. 49

Fig. 8. The seasonal cycle of precipitation over autumn monsoon regions predicted by the model of stable upslope ascent, with the surface specific humidity and wind speed in the direction normal to the slope of the surface that were used as inputs. The y-axes for specific humidity (orange, g/kg) and wind speed (green, m/s) are shown on the right. Regions with downslope winds and therefore negative predicted precipitation were set to zero before spatial averaging, and ocean regions were excluded. The dotted lines indicate the month of maximum climatological precipitation in each region from Figure 2. 50

Fig. 9. The monthly climatologies of precipitation, evaporation, vertically-integrated moisture convergence (VIMC) provided in the reanalysis data, and the VIMC calculated from monthly means from ERA5. The climatological precipitation from TRMM averaged over the same regions is included for comparison.	51
Fig. 10. The climatological annual cycle of the advection, convergence and surface terms calculated in the budget of moisture convergence using ERA5 monthly means for each of the autumn monsoon regions.	52
Fig. 11. The climatological annual cycles of vertical mass flux (colors) and relative humidity as a percentage (contours) averaged over each of the autumn monsoon regions.	53
Fig. 12. The climatological annual cycles of SST and RSST in each of the autumn monsoon regions. The annual-mean SST was subtracted from the climatological values of SST for each region. Panels (a) and (b) are shown with a different y-axis due to the high values of RSST in their annual cycle. The vertical dotted line indicates the month of maximum precipitation over land from Figure 2.	54
Fig. 13. (a) The annual cycle of the tropical-mean SST, averaged between 20°S and 20°N. (b) The difference in climatological SST between autumn and fall, calculated as the September-November mean minus the March-May mean. Negative (blue) values indicate cooler temperatures in boreal autumn.	55

(a) September to February



(b) March to August

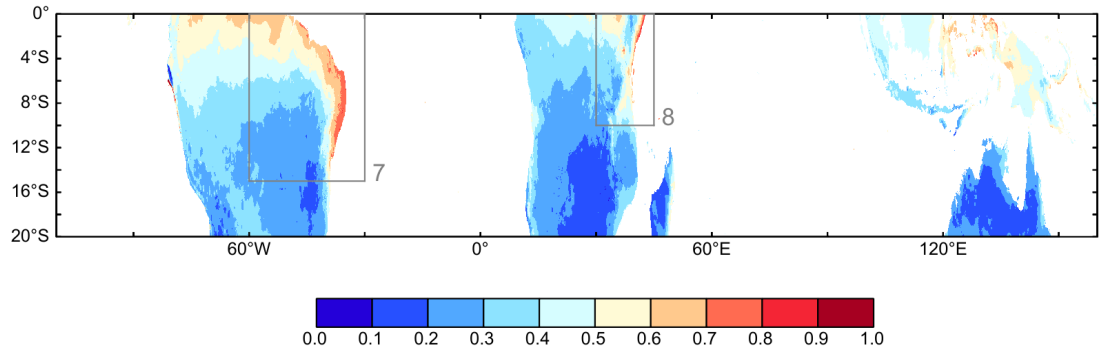


FIG. 1. The climatological fraction of annual rainfall that occurs during the fall and winter months in (a) the Northern Hemisphere (September to February) and (b) the Southern Hemisphere (March to August). Shades of red and orange indicate regions where half or more of the annual rainfall occurs during these months. Gray boxes highlight the eight regions examined in this study, numbered as in the text of Section 3.

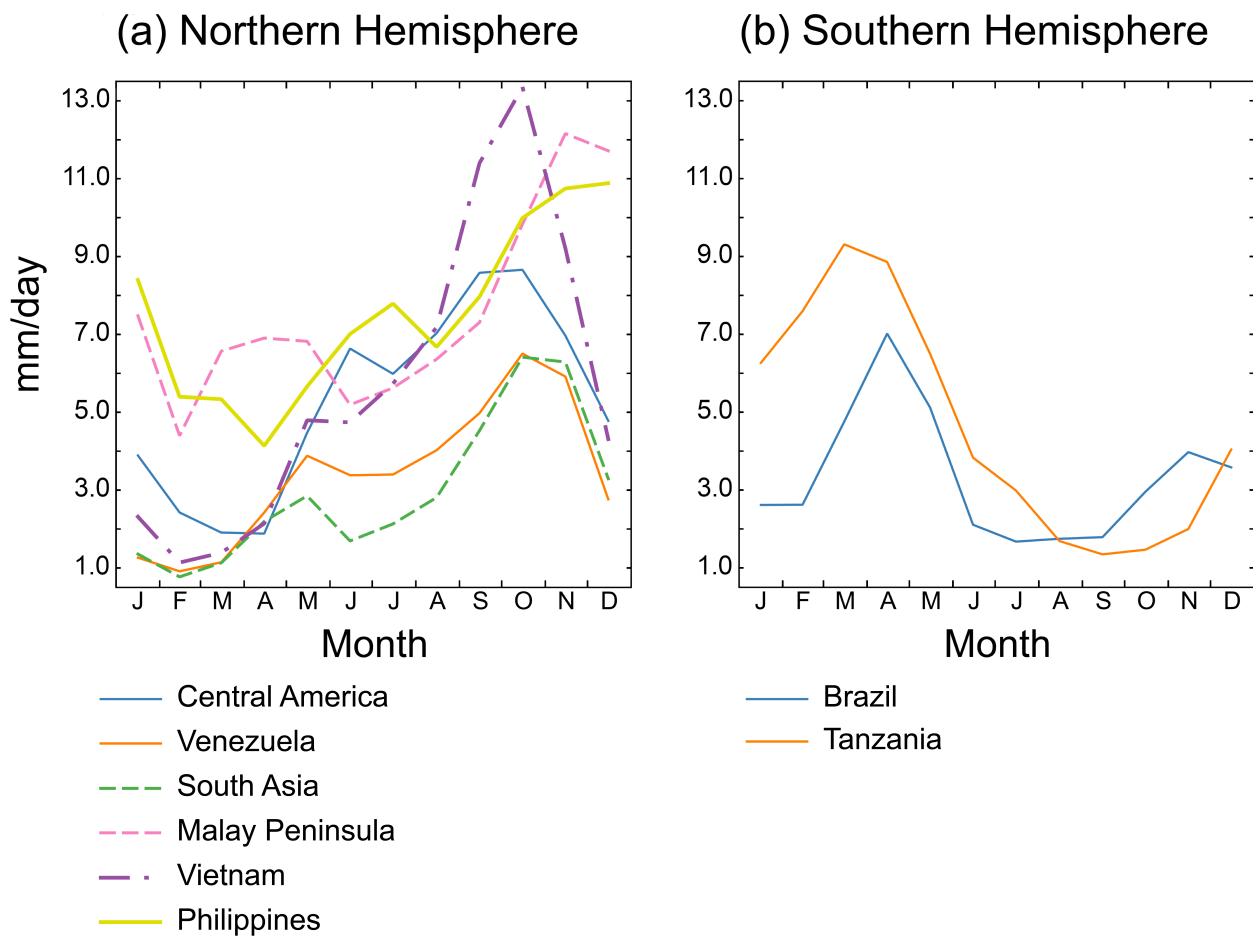
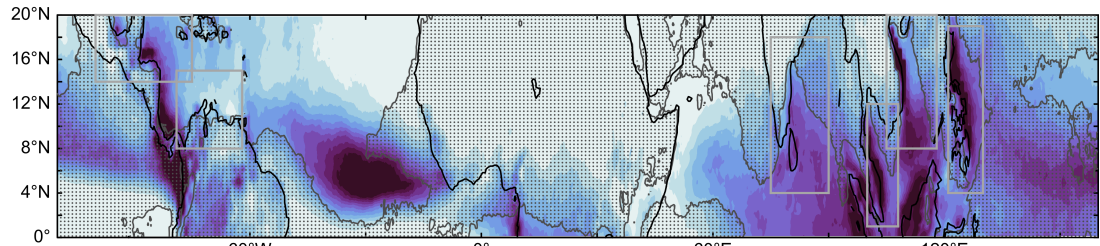


FIG. 2. The climatological annual cycle of precipitation (mm/day) averaged over the areas that receive more than half of their annual rainfall in local autumn and winter in (a) the Northern Hemisphere and (b) the Southern Hemisphere. Spatial averaging was performed over the land areas within the boxes indicated in Figure 1 using CHIRPS data with locations receiving less than half of their annual rainfall in autumn and winter excluded.

(a) October to December



(b) April to June

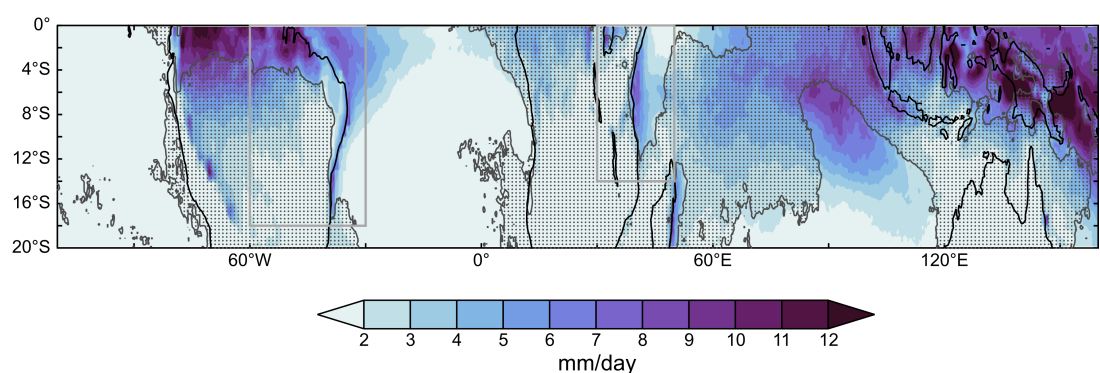


FIG. 3. The climatological precipitation (mm/day) averaged over late autumn and early winter in each hemisphere (October to December in (a) and April to June in (b)) from TRMM. The gray contour demarcates areas that receive more than half of their annual rainfall in local autumn and winter (September to February in (a) and March to August in (b)); regions that receive more than half of their annual rainfall during spring and summer are stippled. Light gray boxes indicate the regions used for averaging in Sections 6 and 7.

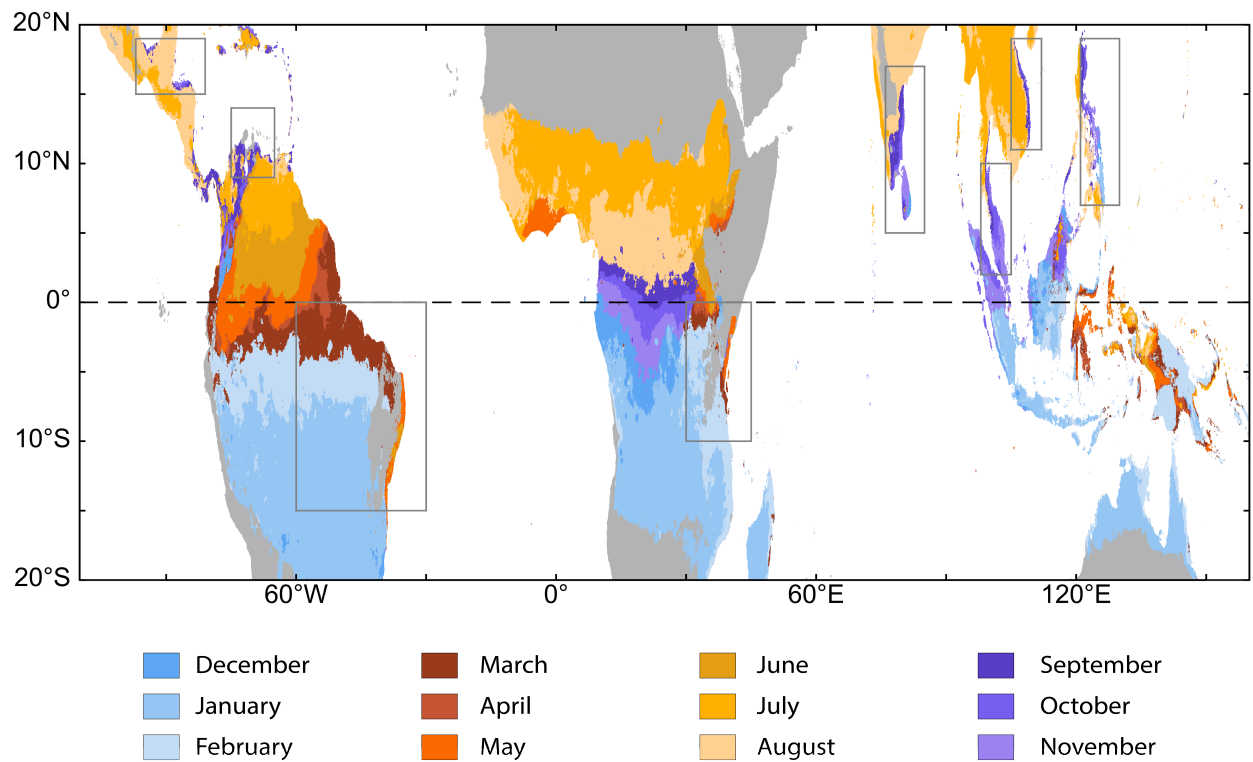


FIG. 4. The climatological month of maximum precipitation at each location from CHIRPS, after a 5-month running mean was applied to the annual cycle. Regions with annual-mean rainfall less than 2 mm/day are indicated in gray.

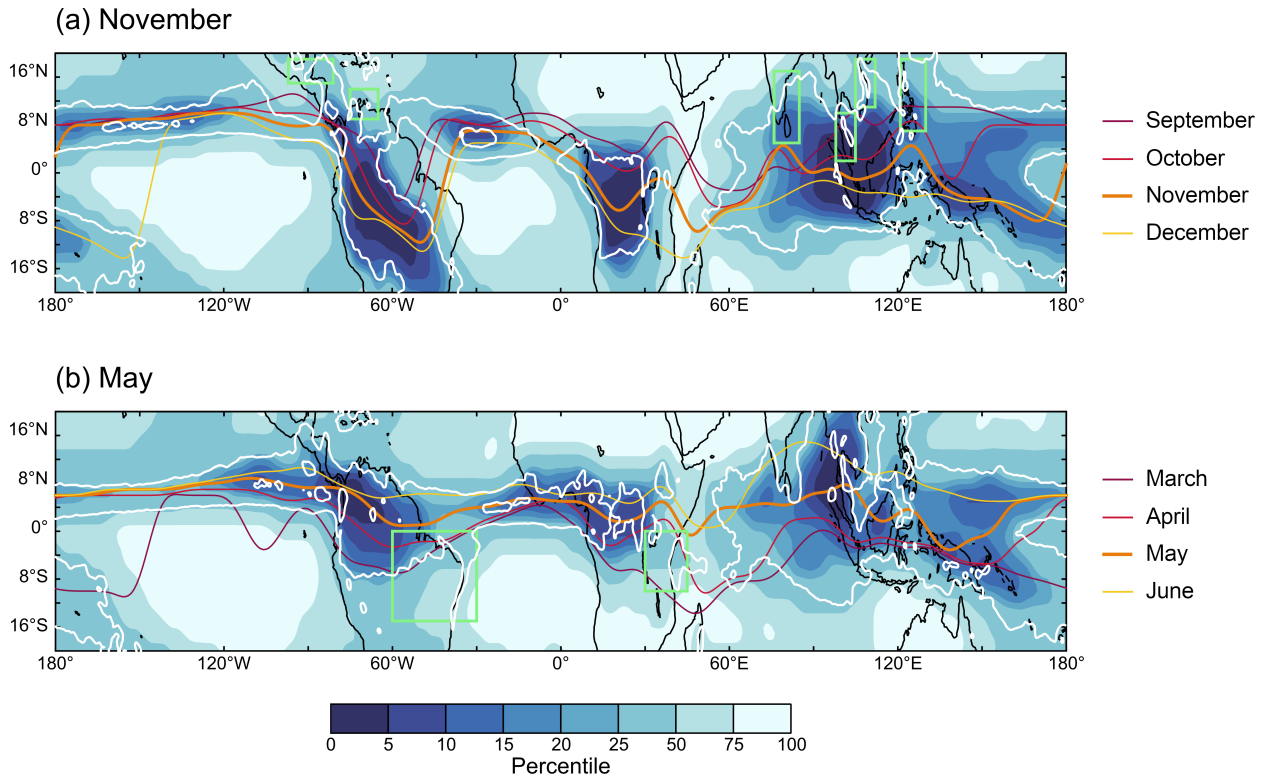
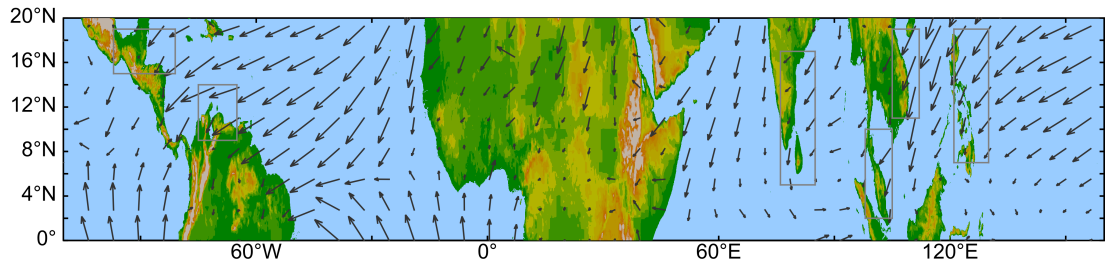


FIG. 5. The percentile of outgoing longwave radiation (OLR) with respect to the climatological distribution of OLR over the tropics in (a) November and (b) May (colors). An uneven color scale is used to highlight the lower percentiles, which suggest convective activity. Contours of 5 mm/day and 15 mm/day of climatological precipitation are shown for the corresponding months in white. Colored lines in panels (a) and (b) indicate the latitude of minimum OLR within the tropics during boreal and austral autumn respectively (see legend), with bold orange lines representing the month for which the other variables in each panel are shown. The latitude of minimum OLR has been smoothed for visualization using a Parzen filter with a window of 7.5° . Green boxes highlight the eight autumn monsoon regions.

(a) October to December



(b) April to June

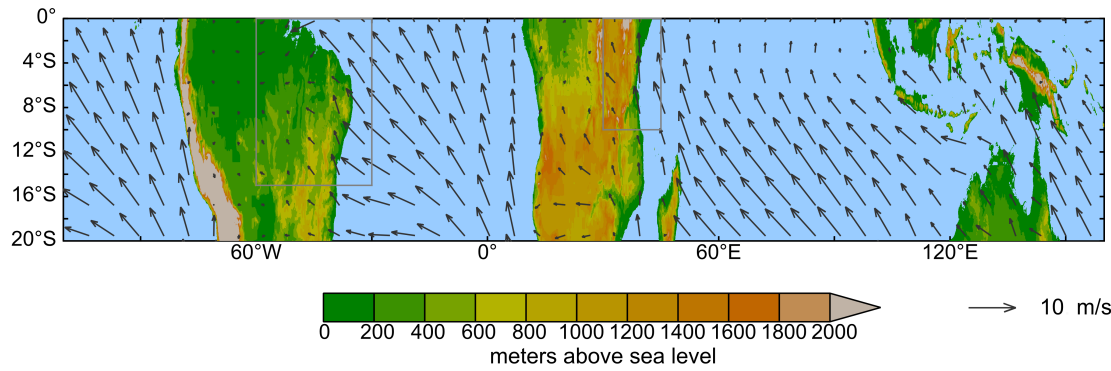


FIG. 6. The height of the land surface above sea level (colors) and the climatological seasonal mean wind field at 10 m above the surface (arrows) in (a) October to December in the Northern Hemisphere and (b) April to June in the Southern Hemisphere.

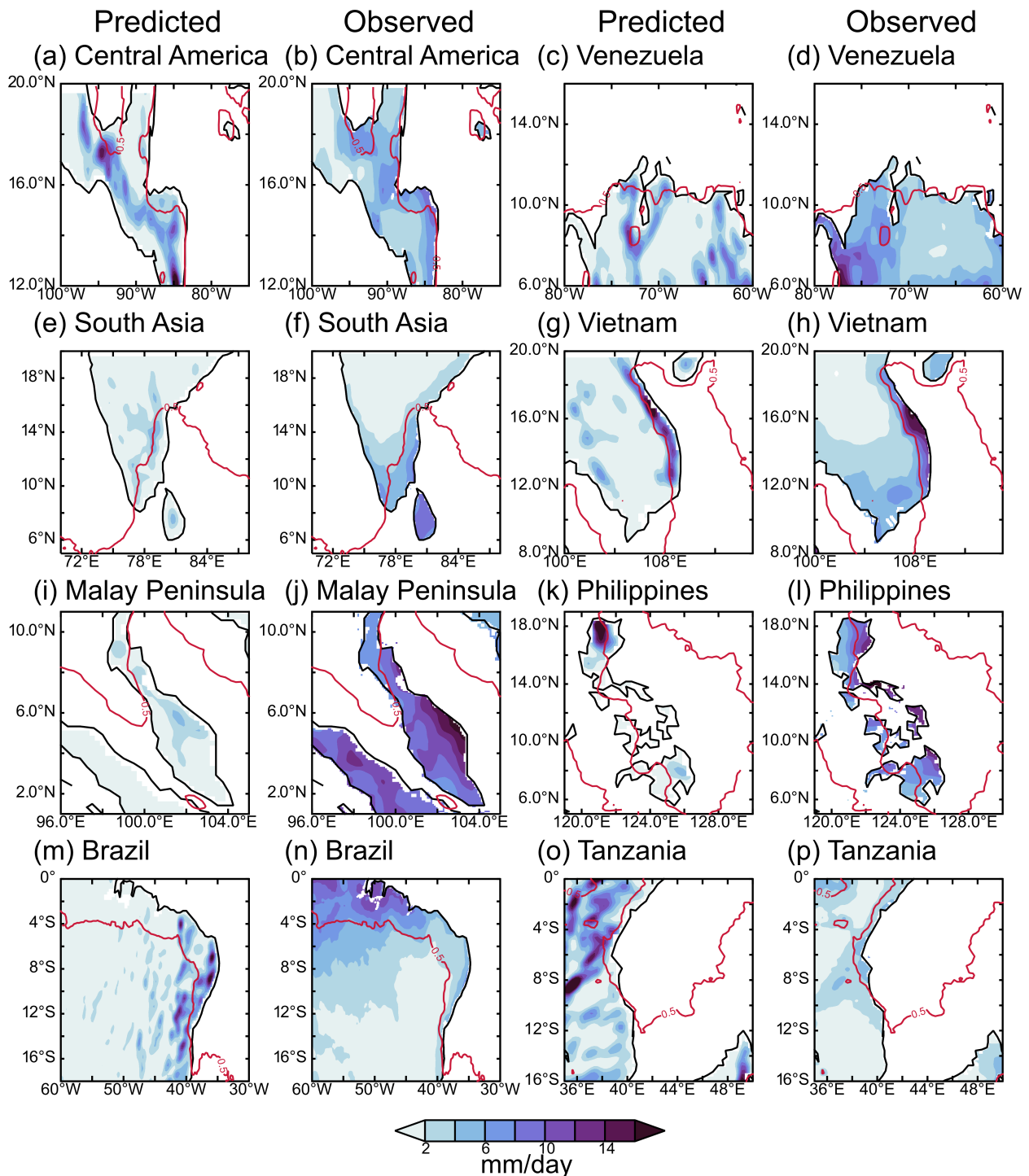


FIG. 7. The climatological precipitation predicted by the orographic model (1st and 3rd columns) and from TRMM (2nd and 4th columns) for comparison in each region, averaged over October–December in the Northern Hemisphere (a–l) and April–June in the Southern Hemisphere (m–p). The red contour demarcates the regions that receive more than half of their annual rainfall in autumn and winter.

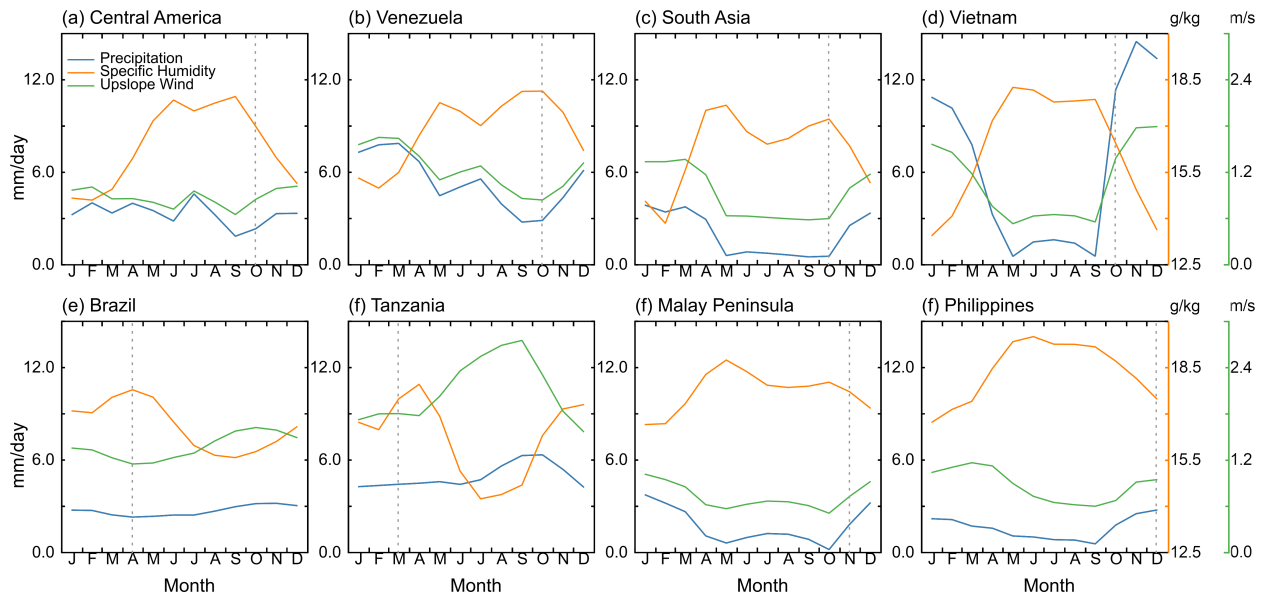


FIG. 8. The seasonal cycle of precipitation over autumn monsoon regions predicted by the model of stable upslope ascent, with the surface specific humidity and wind speed in the direction normal to the slope of the surface that were used as inputs. The y-axes for specific humidity (orange, g/kg) and wind speed (green, m/s) are shown on the right. Regions with downslope winds and therefore negative predicted precipitation were set to zero before spatial averaging, and ocean regions were excluded. The dotted lines indicate the month of maximum climatological precipitation in each region from Figure 2.

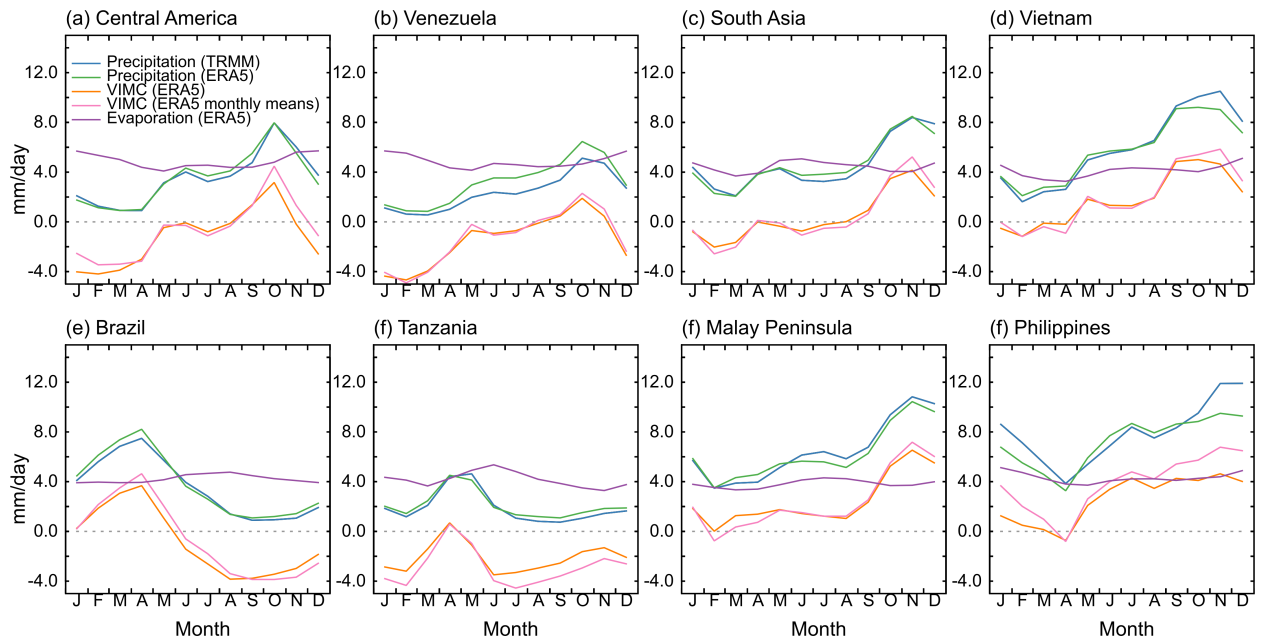


FIG. 9. The monthly climatologies of precipitation, evaporation, vertically-integrated moisture convergence (VIMC) provided in the reanalysis data, and the VIMC calculated from monthly means from ERA5. The climatological precipitation from TRMM averaged over the same regions is included for comparison.

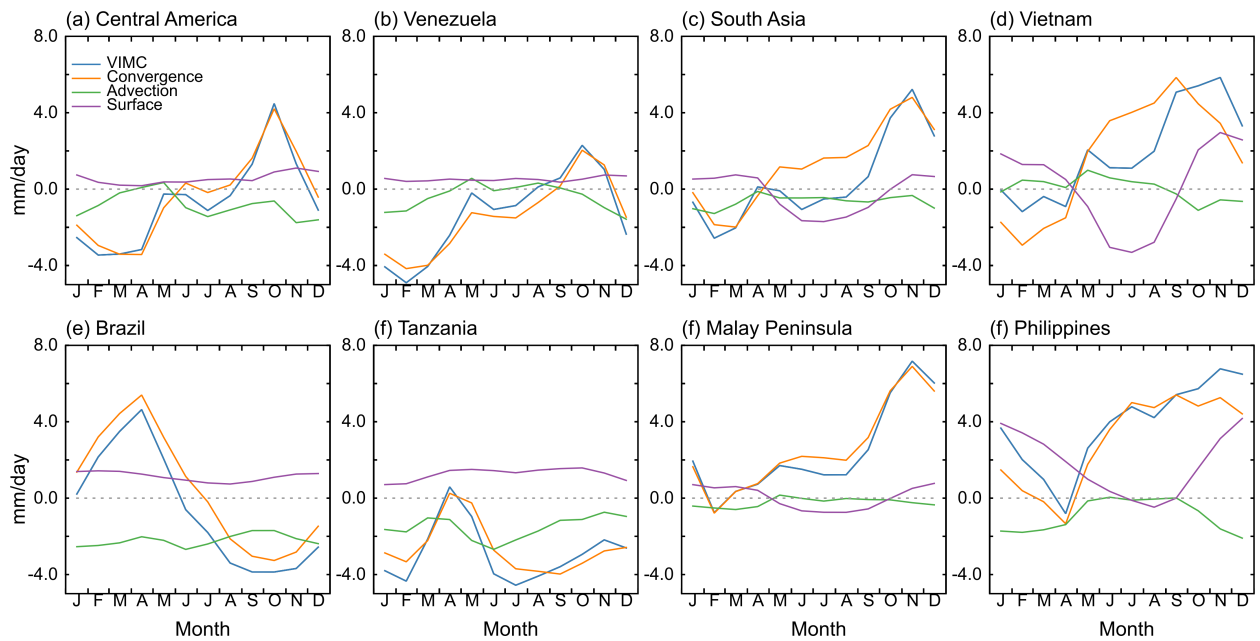


FIG. 10. The climatological annual cycle of the advection, convergence and surface terms calculated in the budget of moisture convergence using ERA5 monthly means for each of the autumn monsoon regions.

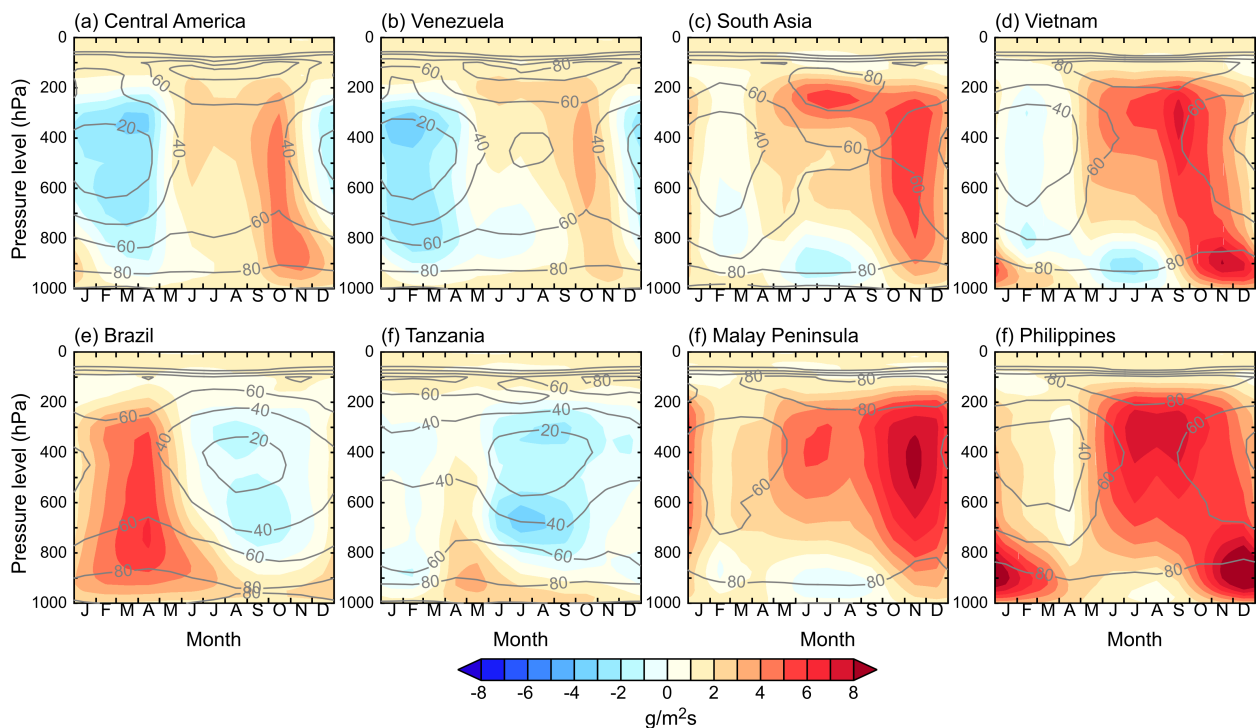


FIG. 11. The climatological annual cycles of vertical mass flux (colors) and relative humidity as a percentage (contours) averaged over each of the autumn monsoon regions.

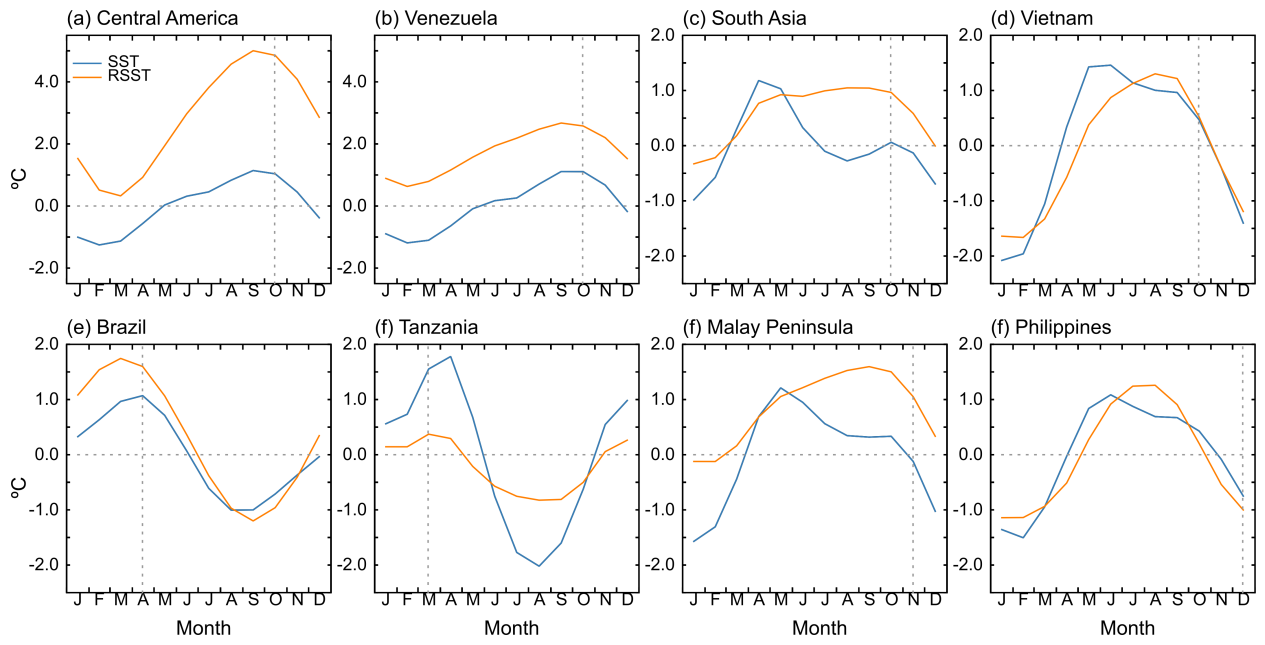


FIG. 12. The climatological annual cycles of SST and RSST in each of the autumn monsoon regions. The annual-mean SST was subtracted from the climatological values of SST for each region. Panels (a) and (b) are shown with a different y-axis due to the high values of RSST in their annual cycle. The vertical dotted line indicates the month of maximum precipitation over land from Figure 2.

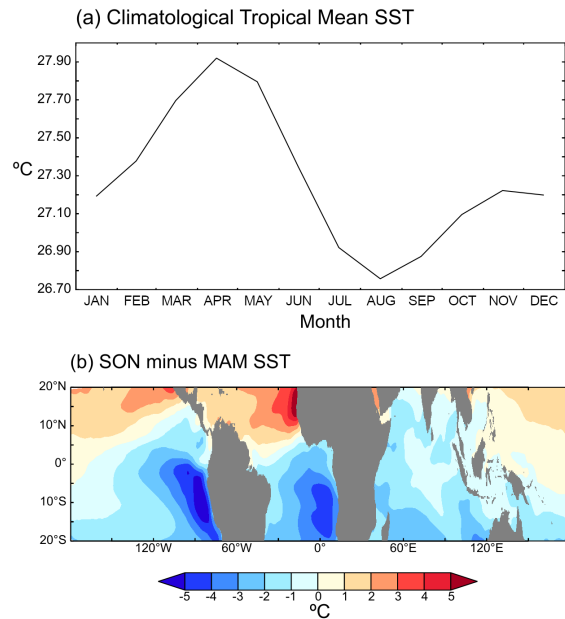


FIG. 13. (a) The annual cycle of the tropical-mean SST, averaged between 20°S and 20°N . (b) The difference in climatological SST between autumn and fall, calculated as the September–November mean minus the March–May mean. Negative (blue) values indicate cooler temperatures in boreal autumn.